Interaction of axonal Chondrolectin with Collagen XIXa1 is necessary for precise neuromuscular junction formation

Article

Cell Reports

Interaction of Axonal Chondrolectin with Collagen XIXa1 Is Necessary for Precise Neuromuscular Junction Formation

Graphical Abstract

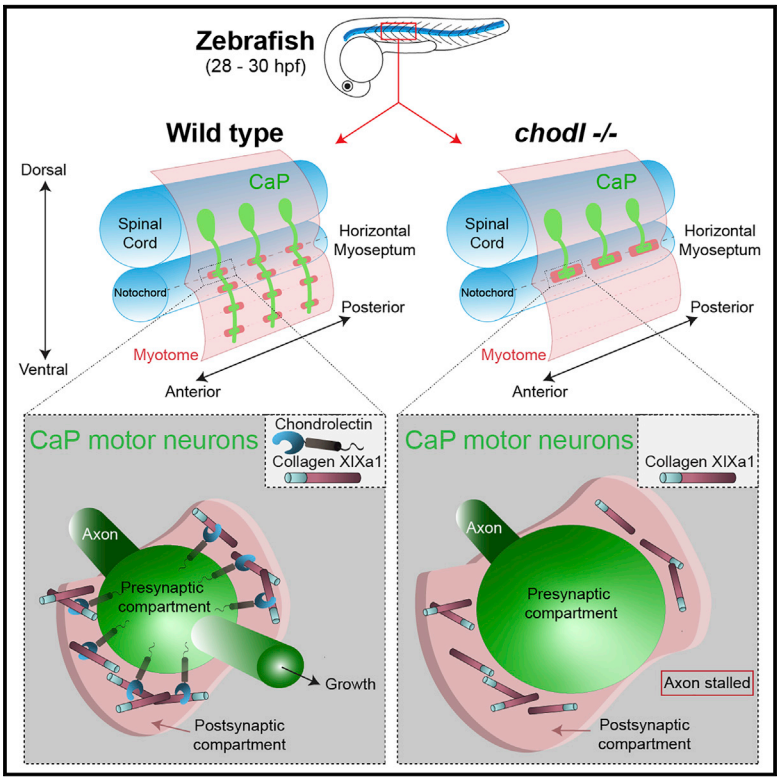

Authors

Ana-Maria Oprişoreanu, Hannah L. Smith, Sukrat Arya, ..., Thomas Becker, Kevin Talbot, Catherina G. Becker

Correspondence

thomas.becker@ed.ac.uk (T.B.), kevin.talbot@ndcn.ox.ac.uk (K.T.), catherina.becker@ed.ac.uk (C.G.B.)

In Brief

The C-type lectin-domain-containing transmembrane molecule Chondrolectin (Chodl) is expressed by motor neurons. Oprişoreanu et al. show that binding of axonal Chodl to extracellular collagen XIXa1 is needed for proper neuromuscular junction differentiation in mice and zebrafish, as well as axon extension and branching at synapses in zebrafish.

Highlights

- Chondrolectin (Chodl) facilitates axon growth and branching at synapses in zebrafish
- *Chodl* restricts neuromuscular junction size across vertebrates
- Lack of *Chodl* alters synaptic transmission
- Chodl binds collagen XIXa1 at the cell surface

Oprişoreanu et al., 2019, Cell Reports *29*, 1082–1098
October 29, 2019
https://doi.org/10.1016/j.celrep.2019.09.033

CellPress

OPEN ACCESS
CellPress

Cell Reports
Article

Interaction of Axonal Chondrolectin with Collagen XIXa1 Is Necessary for Precise Neuromuscular Junction Formation

Ana-Maria Oprişoreanu,[1,5] Hannah L. Smith,[1,5] Sukrat Arya,[3,5] Richard Webster,[3] Zhen Zhong,[1,6] Daniel Wehner,[1,7] Marcos J. Cardozo,[1] Thomas Becker,[1,2,4,8,*] Kevin Talbot,[3,4,*] and Catherina G. Becker[1,2,4,*]

[1]Centre for Discovery Brain Sciences, University of Edinburgh, The Chancellor's Building, 49 Little France Crescent, Edinburgh EH16 4SB, UK
[2]Euan MacDonald Centre for Motor Neurone Disease Research, University of Edinburgh, Edinburgh, UK
[3]Nuffield Department of Clinical Neurosciences, West Wing, John Radcliffe Hospital, University of Oxford, Oxford OX3 9DU, UK
[4]Senior author
[5]These authors contributed equally
[6]Present address: Center for Neuroscience, School of Medicine, Zhejiang University, Hangzhou 310058, People's Republic of China
[7]Present address: Max Planck Institute for the Science of Light, Staudtstraße 2, 91058 Erlangen, Germany
[8]Lead Contact
*Correspondence: thomas.becker@ed.ac.uk (T.B.), kevin.talbot@ndcn.ox.ac.uk (K.T.), catherina.becker@ed.ac.uk (C.G.B.)
https://doi.org/10.1016/j.celrep.2019.09.033

SUMMARY

***Chondrolectin* (*Chodl*) is needed for motor axon extension in zebrafish and is dysregulated in mouse models of spinal muscular atrophy (SMA). However, the mechanistic basis of *Chodl* function is not known. Here, we use *Chodl*-deficient zebrafish and mouse mutants to show that the absence of *Chodl* leads to anatomical and functional defects of the neuromuscular synapse. In zebrafish, the growth of an identified motor axon beyond an "en passant" synapse and later axon branching from synaptic points are impaired, leading to functional deficits. Mechanistically, motor-neuron-autonomous Chodl function depends on its intracellular domain and on binding muscle-derived collagen XIXa1 by its extracellular C-type lectin domain. Our data support evolutionarily conserved roles of *Chodl* in synaptogenesis and provide evidence for a "synapse-first" scenario of motor axon growth in zebrafish.**

INTRODUCTION

In zebrafish, three primary motor axons grow out on a common mid-segmental pathway to the horizontal myoseptum, where axons pause and only the axon of the caudal primary motor neuron (CaP) continues its ventral growth (Beattie et al., 2002; Myers et al., 1986; Westerfield et al., 1986). Although the horizontal myoseptum is a decision point for axon pathfinding, it is also a major synaptic site, where axon growth pauses and axons form the first synapses with so-called muscle pioneers. Contact with the muscle pioneers is not necessary for growth of the CaP axon ventral to the horizontal myoseptum, as shown by ablation of muscle pioneers (Melançon et al., 1997). However, it is unknown whether proper formation of this "en passant" synapse is necessary for the CaP axon's growth cone to be able to escape the contact with muscle pioneers (Beattie et al., 2002; Panzer et al., 2005). Similarly, growth of new axon branches originates from and depends on synaptic points, e.g., in *Xenopus* motor axon arborization (Javaherian and Cline, 2005), arborization of retinal ganglion cell axons in zebrafish (Meyer and Smith, 2006), or the thalamo-cortical projection in mammals (Matsumoto et al., 2016). Hence, both CaP axon extension beyond an en passant synapse and axon branching could depend on synapse stabilization in zebrafish, whereas in mammals, motor axon growth mostly precedes terminal synaptogenesis (Sanes and Lichtman, 1999).

Chondrolectin (Chodl) is a cell surface recognition molecule expressed by motor neurons in zebrafish (Zhong et al., 2012) and is selectively expressed in "fast" motor neurons in mice (Enjin et al., 2010). Knock down of *chodl* in zebrafish leads to prolonged stalling of CaP axons at the horizontal myoseptum while leaving axon pathfinding and overall axon growth speed unaffected (Zhong et al., 2012). However, the exact mechanism of Chodl action is unknown.

Chodl is also dysregulated in an spinal muscular atrophy (SMA) mouse model at an early stage, before detectable muscle weakness (Bäumer et al., 2009; Zhang et al., 2008), and is highly expressed in the most vulnerable motor neurons in an amyotrophic lateral sclerosis (ALS) model (Martínez-Silva et al., 2018; Wootz et al., 2010). Overexpression of *chodl* partially rescues motor axon patterning defects observed in a zebrafish SMA model (Sleigh et al., 2014a), suggesting functions of Chodl in motor neuron disease pathology. We hypothesize that, in vertebrates, Chodl is necessary for synaptic differentiation and, thus, drives motor axon growth and arborization in zebrafish.

Here, we show that, in both embryonic zebrafish and postnatal mice, synaptogenesis is specifically impaired in the absence of *chodl*. We demonstrate that Chodl directly interacts with collagen XIX1a (ColXIX1a) in the extracellular matrix to exert its function. Hence, Chodl is essential for proper neuromuscular junction differentiation in vertebrates and necessary for CaP axon extension and motor axon branching in zebrafish.

RESULTS

To determine evolutionarily conserved functions of *chodl*, we analyzed phenotypes of zebrafish and mouse *Chodl* mutants, followed by protein function analysis.

Generation of a Zebrafish *chodl* Mutant

For mutagenesis, we used CRISPR technology on the background of a transgenic reporter line in which GFP is expressed under the regulatory sequences of the *mnx1* gene (also known as *hb9*) to visualize motor neurons (Flanagan-Steet et al., 2005). Injecting three independent guide RNAs (gRNAs) induced exaggerated stalling of the CaP axon at the horizontal myoseptum in a mosaic fashion (Figures S1A and S1C). Using one efficient gRNA (Figure S1D), we generated a stable mutant with a 4-base pair deletion in the open reading frame near the start codon, leading to a predicted STOP in position 10 of the 236-amino-acid-long protein (Figure S1B), preventing translation of C-type lectin and transmembrane domains. Predicted stop codons may lead to non-sense-mediated decay of the RNA (Anderson et al., 2017). Indeed, mRNA expression was reduced by a third in qRT-PCR (Figures S1G, S1I, and S1J). However, potentially truncated forms of the protein could still exist. Homozygous mutants were adult viable and did not show alterations of body size, eye size, or muscle development in embryos (Figures S1E and S1F). In contrast, 73% (99 of 136 motor axons in 17 embryos) of motor axons were stalled at the horizontal myoseptum at 28 h post fertilization (hpf), whereas in wild-type embryos, all axons (128 of 128 motor axons in 16 embryos) had grown beyond that point (data not shown). Axons were always assessed on one side of the embryo in segments 7–14. In a different set of embryos, motor axon length was reduced by 58% in the mutant (Figures 1A and 1B). Middle primary motor neuron (MiP) axons were also shorter in the mutant (Figures S1K–S1M). This replicates the *chodl* morpholino phenotype (Zhong et al., 2012) and confirms that we generated a *chodl* zebrafish mutant with disrupted gene function.

Correct Gene Expression Level of *chodl* Is Required in Zebrafish Motor Neurons

Next, we addressed whether stalling of CaP axons at the horizontal myoseptum in *chodl* mutants was motor neuron autonomous and whether the introduced mutation led to a loss of gene function. To that aim, we generated a transgenic line on the background of the *chodl* mutant (with *mnx1*:GFP transgene) that selectively overexpressed FLAG-tagged *chodl* in motor neurons under the regulatory sequences of *mnx1*. Overlap of FLAG-tag immunoreactivity and GFP signal in *mnx1*:GFP transgenic animals confirmed correct targeting (Figure 1A). In this line, designated (*chodl−/−; mnx1:chodl-FLAG*), the stalled axon phenotype was completely rescued (Figures 1A and 1B). Hence, the short CaP axon phenotype is a loss-of-function mutation and is cell autonomous for motor neurons.

To determine if excess *chodl* expression in motor neurons altered axon growth, we injected the *mnx1*:*chodl*-FLAG construct into wild-type zygotes. This adds additional *chodl* expression to the wild-type levels. At 28 hpf, *chodl*-FLAG-expressing axons were reduced in length by 39% compared to vector-injected control axons and by 39% compared to FLAG-negative axons in the same animals, as an internal negative control. (Figures 1C and 1D). Although relatively few embryos showed transfected CaP neurons, statistical power was 0.999, indicating robustness of results. The same was true when CaPs were considered individually (Figure S1H). Therefore, both increased and reduced levels of *chodl* expression in motor neurons impair axon growth in a cell-autonomous manner.

Lack of *chodl* Impairs Synaptogenesis during Early CaP Axon Growth

Lack of *chodl* only affects CaP axon growth by prolonging stalling at the horizontal myoseptum, a major synaptic site with muscle pioneers (Zhong et al., 2012). Synaptic sites may be important for the growth of exploratory filopodia and as a starting point for axon branching (Javaherian and Cline, 2005; Panzer et al., 2006). We tested whether filopodia dynamics were altered for CaP axons by using video time-lapse microscopy of CaP growth cones at the horizontal myoseptum. Filopodia, visualized with the F-actin binding Lifeact peptide (Riedl et al., 2008), were not changed in number and average survival time in the mutant (Figures S2A–S2E). Hence, a lack of *chodl* does not detectably affect filopodia dynamics.

Next, we tested whether synaptogenesis would be affected in the *chodl* mutant. Analyzing the horizontal myoseptum synaptic site with the Znp-1 antibody to the pre-synaptic protein Synaptotagmin 2 (Syt2) (Wen et al., 2010) at 28–29 hpf, we found that the total area of Syt2 immunoreactivity was enlarged by 30% in the mutant compared to wild-type controls (Figures 2A and 2B). As an additional measure of pre-synaptic differentiation, we determined whether immuno-reactivity clustered into appropriate puncta. Puncta were defined as distinct structures of high immunoreactivity for pre-synaptic, post-synaptic, or both markers. Instead of forming discernible pre-synaptic puncta at the horizontal myoseptum (2.61 puncta/hemisegment in controls), enlarged puncta were not clearly separated from each other, leading to the detection of fewer of these in the mutant (1.55 puncta/hemisegment; Figure 2E). Intensity of immunoreactivity was also increased by 57% in the mutant (Figure 2H). All of these parameters were rescued to wild-type levels in the (*chodl−/−; mnx1:chodl-FLAG*) line (Figures 2B, 2E, and 2H).

Using antibodies to Synaptic Vesicle glycoprotein 2 (SV2) to label the pre-synaptic area, we found no change in total area but saw a similar reduction in the number of discernible puncta per hemisegment that was rescued in the (*chodl−/−; mnx1:chodl-FLAG*) line (Figures S3A–S3C). Hence, differentiation of pre-synaptic structures is disrupted by a lack of Chodl in motor neurons.

The total post-synaptic area, labeled with antibodies to acetylcholine receptors (anti-AChR), was not significantly altered in *chodl* mutants (Figure 2C). However, the number of discernible post-synaptic AChR^{+} puncta was reduced from 3.98 puncta/hemisegment in controls to 2.84 in mutants and rescued in the (*chodl−/−*; *mnx1*:Chodl-FLAG) line (Figure 2F). The labeling intensity of AChR was not affected in the mutant but was 16% lower in the (*chodl−/−; mnx1:chodl-FLAG*) line than in controls (Figure 2I), perhaps due to inadequate levels of Chodl being achieved in the rescue line. Overall, this means that clustering

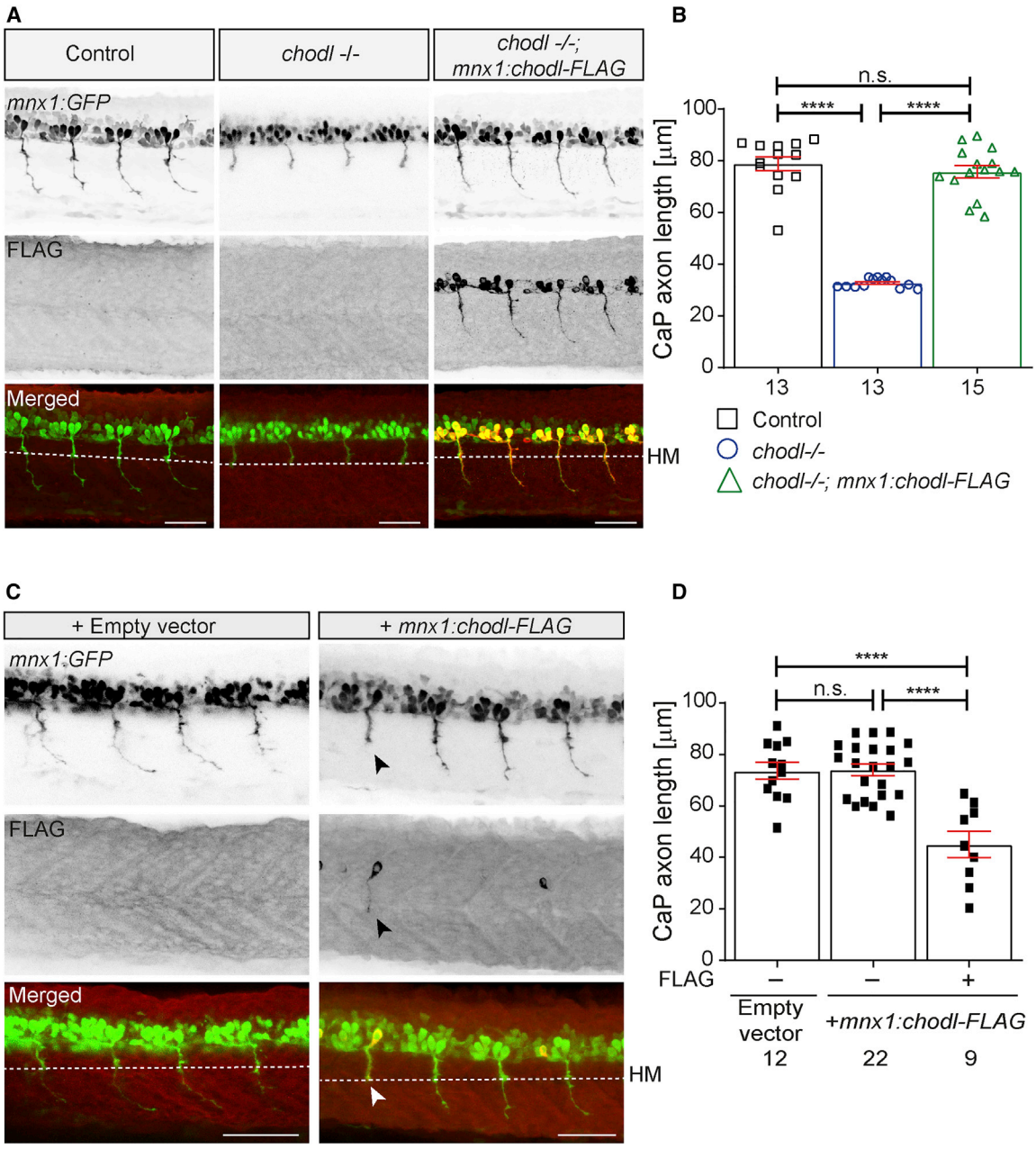

Figure 1. Precise Levels of Chodl Are Needed in CaP Motor Neurons for Unimpeded Axon Growth

Lateral trunk views of zebrafish embryos at 28 hpf are shown. Dashed lines indicate the horizontal myoseptum (HM).

(A) Motor axons are stalled at the horizontal myoseptum in *chodl* mutants. Axon length is restored by stable transgenic expression of FLAG-tagged Chodl in motor neurons of mutants in the (*chodl−/−; mnx1:chodl-FLAG*) line.

(B) Quantification of axon lengths of F2 (*chodl−/−; mnx1:chodl-FLAG*) embryos without FLAG immuno-histochemistry are shown (****$p < 0.0001$; statistical power = 1.00).

(C) Acute, mosaic expression of *mnx1*:chodl-FLAG in wild-type embryos leads to reduced growth of $FLAG^+$ (arrowhead in C) but not $FLAG^-$ axons in the same embryos or in embryos injected with the empty vector.

(D) Quantification of CaP axon length from mosaic expression of *mnx1*:chodl-FLAG in wild-type embryos (****$p < 0.0001$; statistical power = 0.999).

Scale bars, 50 µm; each data point represents one animal; data are represented as mean ± SEM; n.s., not significant.

See also Figures S1 and S2.

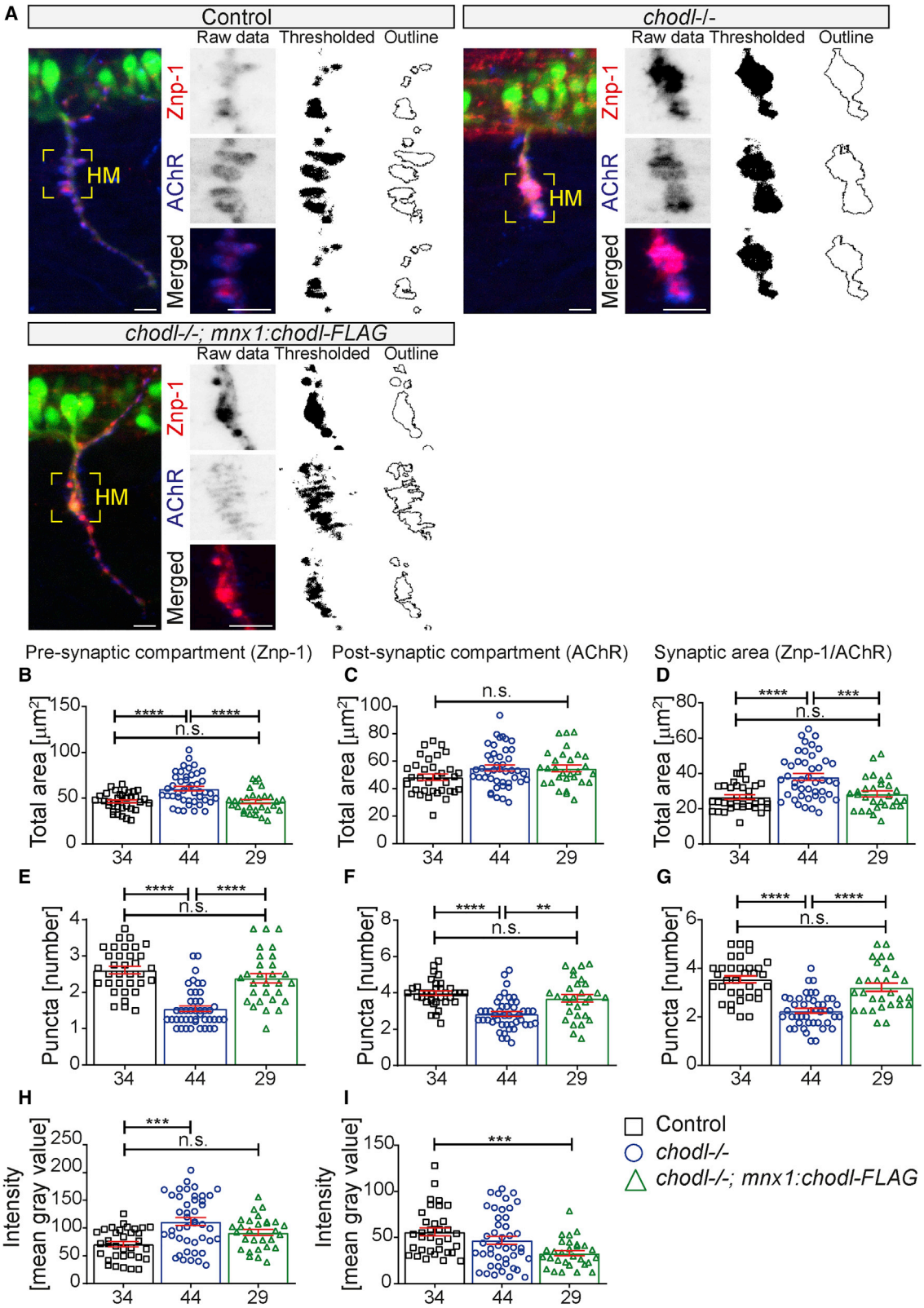

(legend on next page)

of post-synaptic AChR$^+$ puncta is affected by a lack of pre-synaptic Chodl.

To determine the synaptic area, we measured the overlap of pre-synaptic (anti-Syt2) and post-synaptic (anti-AChR) labeling. The total synaptic area was increased by 42% in the mutant, and the number of discernible synaptic puncta per hemisegment was decreased from 3.55 to 2.24. Both measurements were rescued in the (*chodl−/−; mnx1:chodl-FLAG*) line (Figures 2D and 2G). Hence, mutating *chodl* in motor axons disrupts synaptic differentiation on muscle pioneers at the horizontal myoseptum.

Next, we asked whether synapse maturation was only delayed in *chodl* mutants or whether defects persisted even when the axons had grown beyond the horizontal myoseptum. In older embryos (31 hpf), we analyzed the synaptic phenotype only in hemisegments with axons that had grown beyond the horizontal myoseptum in the mutant. Pre-synaptic labeling area (anti-Syt2) was not increased, but the number of discernible puncta per hemisegment was reduced from 2.91 to 2.14 (Figures S3G, S3H, and S3L), and the labeling intensity was increased (by 58%; Figure S3K) compared to wild-type controls. Anti-SV2 labeling showed an increased total pre-synaptic area and reduced number of discernible puncta per axon (Figures S3D–S3F).

Post-synaptic labeling of AChR showed no changes in total area and discernible cluster number per hemisegment but showed a slightly increased labeling intensity by 22% (Figures S3I, S3M, and S3O). The synaptic area was increased by 51%, and the number of discernible synaptic puncta per hemisegment was reduced from 3.60 to 2.66 (Figures S3J and S3N). Hence, similar pre-and post-synaptic aberrations and an increase of synaptic area were present at the horizontal myoseptum for axons stalled at the horizontal myoseptum and those that had grown beyond this point. This suggests that eventual "escape" of CaP axons from the horizontal myoseptum is not associated with full normalization of synapse morphology.

Lack of *chodl* Impairs Axon Branching in Zebrafish

After 48 hpf, motor axons branch onto the muscle, and it has been shown in *Xenopus* that this depends on synapse formation (Javaherian and Cline, 2005). Axons only form new branches at synaptic sites in *Xenopus*. Analyzing axon branching onto myotomes at 3 dpf in zebrafish, we find that 97% of axonal branch points coincide with synaptic puncta (429 of 443 branch points in 10 larvae; Figures S4A and S4B), suggesting similar mechanisms in zebrafish. Therefore, we hypothesized that in *chodl* mutants, axon branching and synaptogenesis onto the myotomes should be impaired.

We analyzed axon branching and synapse formation in *chodl* mutants at 3 dpf, when motor axons are highly branched over the myotomal surface in wild-type animals. Mid-segmental nerve trunks were present in *chodl* mutants but showed strongly reduced branching on the muscle tissue (Figure 3A). To quantify myotomal innervation, we labeled synaptic puncta, defined as puncta of AChR immuno-reactivity with an overlying SV2$^+$ puncta (Figures 3B–3J). The number of synaptic puncta on the muscle surface in the mutant was reduced by 72.5%. This was partially rescued in the (*chodl−/−; mnx1:chodl-FLAG*) line, with a reduction by 26.1%, compared to synapse numbers observed in wild-type control animals (Figure 3K). Overall, *chodl* mutants show an axon-autonomous impairment of axon branching and synaptogenesis on the muscle tissue. Muscle pioneers, the first muscle cells the CaP axon forms synapses with, develop into slow muscle fibers. That process is complete at 2 to 3 weeks of development (Devoto et al., 1996). Hence, we cannot assess the specific roles of *chodl* for fast versus slow muscle fibers in zebrafish from the above data on the immature system.

The Touch-Evoked Escape Response Is Impaired in Zebrafish Larvae

The earliest motor axon/muscle interactions take place at 18–19 hpf, before CaP axons reach the horizontal myoseptum. At this time point, coiling behavior occurred at a frequency that was unaltered in *chodl* mutants compared to wild-type embryos (Figure S4C). This indicates the absence of an early movement phenotype in *chodl* mutants.

To determine whether the observed axonal branching phenotypes are correlated with behavioral deficits, we used a touch assay to quantify escape reactions of larvae at 3 dpf. Despite hypo-innervation of trunk musculature, larvae swam the same distance after touching their tail (Figures S4D and S4E). However, high-speed analysis of the C-bend turning reaction after a head touch (Figure 3L) indicated that the initial escape angle of *chodl* mutants was reduced from 144 to 105 degrees, resulting

Figure 2. CaP Axons of *chodl* Mutants Show Pre- and Post-Synaptic Defects at the Horizontal Myoseptum

(A) Motor neurons of *mnx1*:GFP transgenic animals are green. Znp-1 antibody labels the pre-synapse and AChR the post-synapse. Yellow squares indicate the measurement areas. Scale bar, 10 μm.

(B and E) Pre-synaptic puncta at the horizontal myoseptum (HM) are enlarged (B, total area) and fewer individual puncta can be identified in the *chodl* mutant (E; discernible puncta). These parameters are rescued in the (*chodl−/−; mnx1:chodl-FLAG*) line (B, ****p < 0.0001, statistical power = 1.00; E, ****p < 0.0001; statistical power = 0.9977).

(C and F) Post-synaptic puncta area at the horizontal myoseptum is unchanged (C, total area), but fewer individual puncta are detected in the *chodl* mutant compared to wild-type animals (F; discernible puncta). This parameter is rescued in the (*chodl−/−; mnx1:chodl-FLAG*) line. (****p < 0.0001, **p = 0.0012; statistical power = 0.9996).

(D) Synaptic area is increased in the mutant and rescued in in the (*chodl−/−; mnx1:chodl-FLAG*) line (****p < 0.0001, ***p = 0.0005; statistical power = 0.9978).

(G) The number of discernible synaptic puncta is reduced in the mutant and rescued in the (*chodl−/−; mnx1:chodl-FLAG*) line (****p < 0.0001; statistical power = 0.999).

(H) Intensity of Znp-1 labeling is increased in *chodl* mutants compared to wild-type control and the (*chodl−/−; mnx1:chodl-FLAG*) line (***p = 0.0002; statistical power = 0.9918).

(I) The mean intensity of AChR labeling is decreased the (*chodl−/−; mnx1:chodl-FLAG*) line compared to wild-type control and *chodl* mutants (***p = 0.0010; statistical power = 0.9097).

Each data point represents one animal; data are represented as mean ± SEM; n.s., not significant.

See also Figure S3.

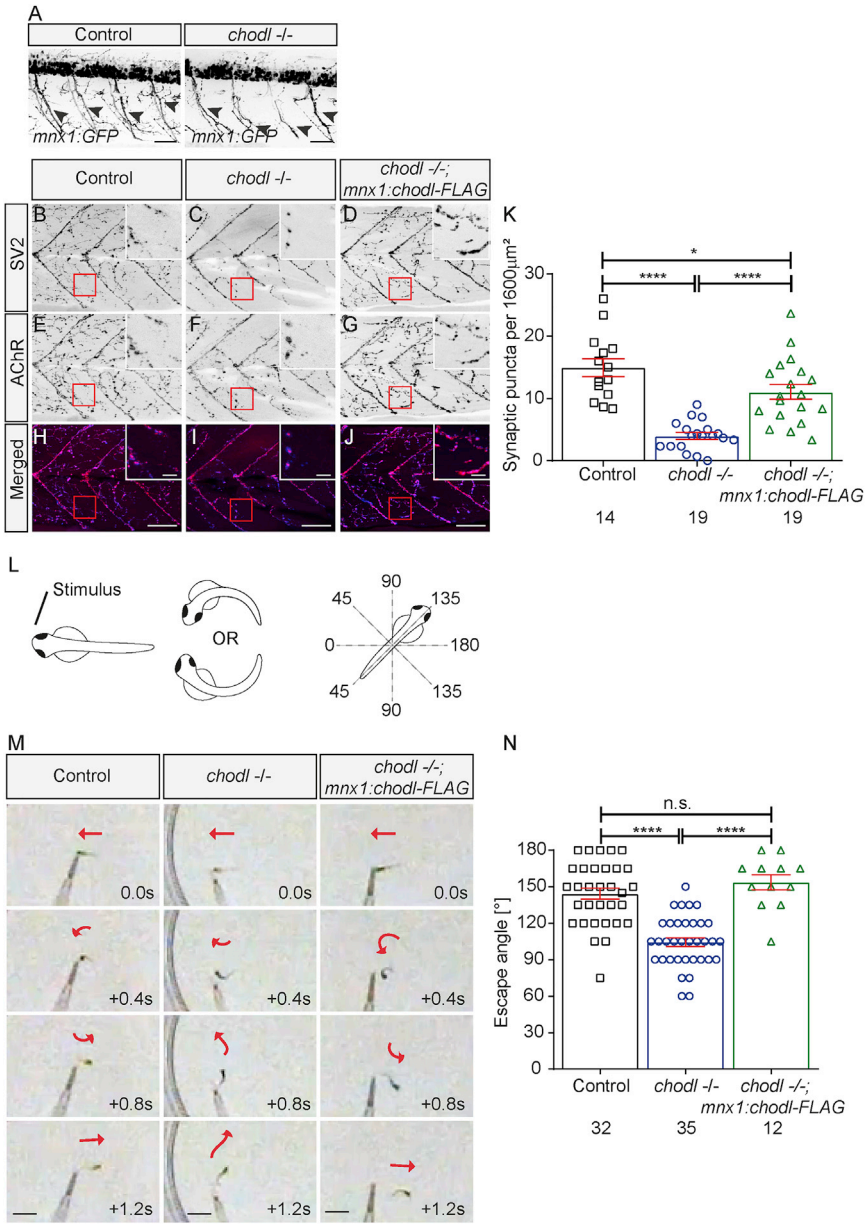

Figure 3. Chodl Is Necessary for Axon Branching onto the Myotome Surface and Proper Escape Response

Lateral trunk views are shown.

(A) *mnx1*:GFP^{+} motor nerves are present along the mid-segmental pathway (ventral motor nerves, black arrowheads) but lack branching onto the myotome in *chodl* mutants at 3 dpf.

(B) SV2 immunohistochemistry in wild-type zebrafish.

(C) SV2 immunohistochemistry in *chodl* mutant.

(D) SV2 immunohistochemistry in the (*chodl*−/−; *mnx1:chodl-FLAG*) line is shown.

(E) AChR immunohistochemistry in wild-type zebrafish is shown.

(F) AChR immunohistochemistry in the *chodl* mutant is shown.

(G) AChR immunohistochemistry in the (*chodl*−/−; *mnx1:chodl-FLAG*) line is shown.

(H) Overlap of SV2 and AchR labeling in wild-type zebrafish is shown.

(I) Overlap of SV2 and AchR labeling in *chodl* mutant is shown.

(J) Overlap of SV2 and AchR labeling in (*chodl*−/−; *mnx1:chodl-FLAG*) line is shown. The density of synapses (overlap of SV2 and AChR labeling) on the surface of the myotomes is reduced in *chodl* mutants compared to controls and is partially rescued in the *chodl-FLAG* rescue line. Regions of analysis (red boxes) are shown in higher magnification as insets.

(K) The number of synapses is reduced in *chodl*−/− larvae compared to controls and partially rescued in the (*chodl*−/−; *mnx1:chodl-FLAG*) line (****$p < 0.0001$, *$p = 0.0419$; statistical power = 0.9999). Scale bars, 50 µm. Insets scale bar, 10 µm.

(L) Cartoon shows starting position of the larvae and the C-bend, which can be randomly to the left or right after tapping the head and the angle is measured.

(M) Representative frames of high-speed recording of the touch-evoked escape response are shown for wild-type control, *chodl* mutants, and (*chodl*−/−; *mnx1:chodl-FLAG*) animals. Turning movements of larvae are indicated by red arrows (arrowhead indicates head). Scale bars, 4 mm.

(N) The turning angle is reduced in mutant larvae, compared to wild-type animals and rescued in the *chodl*−/−; *mnx1*:chodl-FLAG line. (****$p < 0.0001$; statistical power = 1.00)

n.s., not significant; each data point represents one animal; data are represented as mean ± SEM. See also Figure S4.

in inefficient escape from the stimulus. In (*chodl*−/−; *mnx1:chodl-FLAG*) animals, this defect was fully rescued (Figures 3M and 3N), suggesting specificity of the phenotype for motor neurons. However, we cannot exclude a contribution from *chodl* (http://zfin.org) and *mnx1* (Korzh et al., 2011) co-expressing hindbrain neurons to the phenotype. In summary, a lack of *chodl* impairs neuromuscular synaptogenesis, as well as axon growth and branching, leading to specific aberrations in swimming behavior.

Characterization of *Chodl* Mutant Mice

To determine conserved functions of *Chodl* in mammals, we analyzed a CRISPR-generated mouse mutant (see STAR Methods). The mutant carries a 576-nucleotide deletion. This removes exon 2, present in all known protein-coding isoforms (Ensembl: Chodl-201 ENSMUST00000023568.13, Chodl-202 ENSMUST00000069148.12, Chodl-203 ENSMUST00000114216.1, and Chodl-205 ENSMUST00000232415.1; Figure S5A). RT-PCR confirmed that *Chodl* exon 2 was not expressed

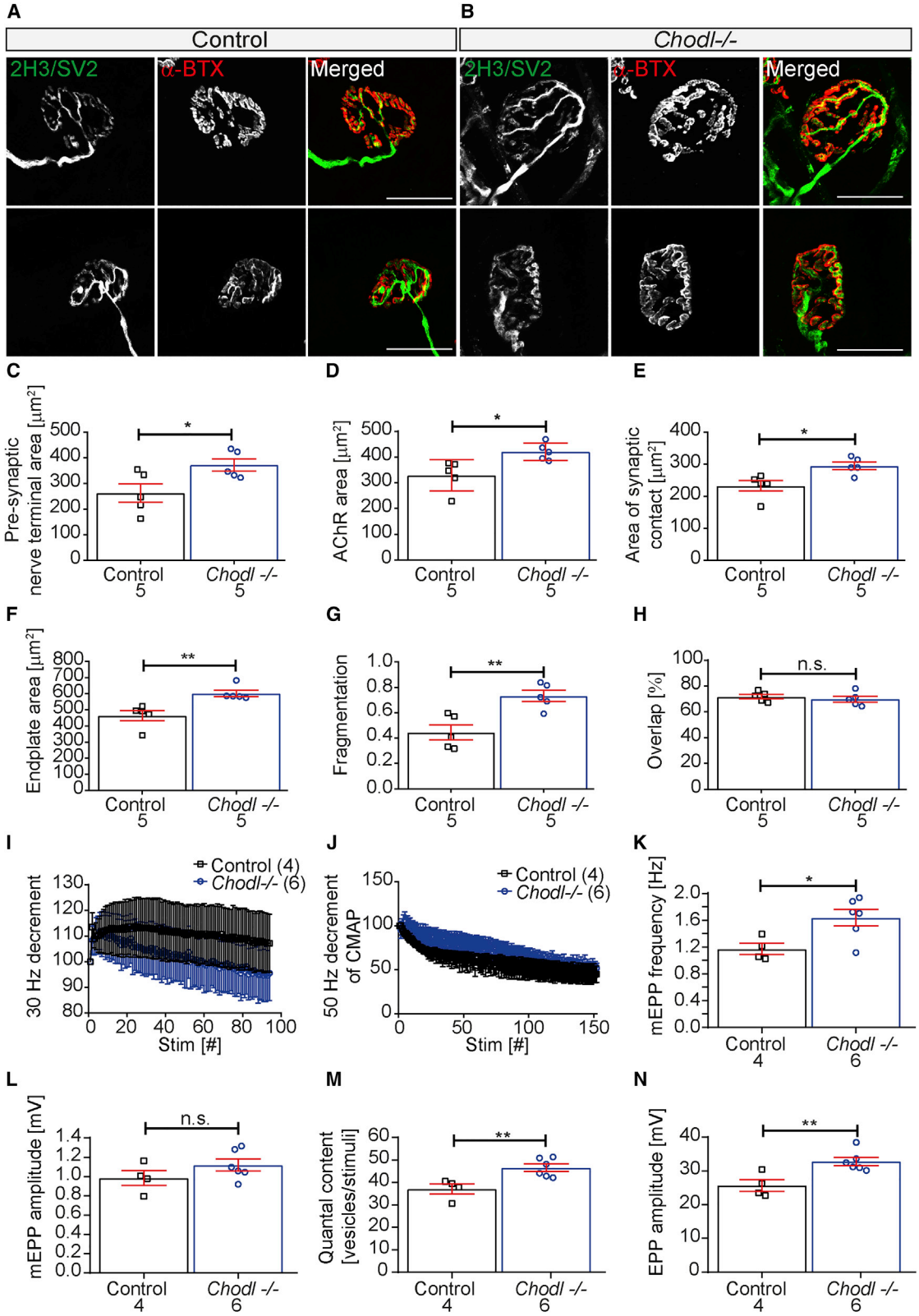

(legend on next page)

(Figure S5B). *Chodl* homozygous and heterozygous mutant mice were viable, with no reduction in expected progeny for each genotype (Figure S5C).

The removed exon 2 codes for most of the C-type lectin domain, which is essential for the function of the protein (see below). Moreover, removal of exon 2 induces a frameshift and is predicted to produce a premature stop codon in all protein-coding isoforms and, hence, mutant mice that lack *Chodl* function.

Lack of *Chodl* Function Impairs Neurite Growth in Cultured Mouse Motor Neurons

We investigated the neuronal function of *Chodl* by characterizing neurite outgrowth of motor neurons (MNs) cultured from embryonic day 13.5 (E13.5) mouse spinal cord on Laminin. There was a reduction in overall neurite length (by 31.87%) and number of Tuj1-labeled neurite branches (by 23.39%) of Islet-1^{+} neurons (Figures S5D–S5G). Cell body size was not altered (Figure S5H). This may be due to a reduced intrinsic growth capacity of *Chodl* mutant axons or interactions of Chodl with Laminin *in vitro*.

Synaptogenesis Is Impaired in *Chodl* Mutant Mice

The number of choline acetyltransferase (ChAT)-positive neurons at spinal level L1–L2 in the ventral horn of 4-month-old wild-type and *Chodl* mutant mice did not differ (Figures S6A–S6C). Terminal branching of motor nerves, which does not coincide with synaptogenesis at the branch points as in zebrafish, was not affected in the mutant (Figures S6D and S6E), supporting that *Chodl* deficiency does not affect axon growth and branching *in vivo*.

To assess synaptic phenotypes, we determined neuromuscular junction morphology by using immunohistochemistry. The lumbrical muscles of 4-month-old mice were analyzed because they are thin and flat enough to be mounted intact. These muscles are innervated by *Chodl*$^{+}$ "fast" motor neurons (Enjin et al., 2010). The neuromuscular junctions were labeled with a mix of antibodies to neurofilament (2H3; axons) and SV2 (pre-synapse) and fluorescently tagged α-bungarotoxin (α-BTX; post-synapse).

The pre-synaptic area was increased by 41% in *Chodl* mutant mice, the post-synaptic area by 28%, and the area of synaptic contact by 27%, compared to wild-type animals at 4 months of age (Figures 4A–4E). The shape of synapses was changed, as the area taken by individual synapses, the endplate area, was increased by 30% (Figure 4F). Moreover, endplate labeling in *Chodl* mutants was more fragmented, showing a fragmentation index (Jones et al., 2016) of 0.73, compared to 0.45 in wild-type animals (Figure 4G).

To find indications of potential synapse degeneration, we determined the proportion of post-synaptic sites that were not occupied by pre-synaptic terminals. The percentage of innervated post-synaptic area ("overlap") was similar in 4-month-old mutant and wild-type animals (Figure 4H), indicating that there was no sign of neuromuscular junction denervation. Hence, *Chodl* mutant mice show an enlargement of the synaptic area that is similar to that seen in zebrafish embryos.

The Endplate Potential Amplitude Is Increased in the Absence of *Chodl* in Mice

To test the function of neuromuscular synapses in *Chodl* mutant mice, we measured the compound muscle action potential (CMAP) in a phrenic-nerve-diaphragm-muscle preparation. The phrenic nerve of wild-type, but not *Chodl* mutant animals contains *Chodl* mRNA, as shown by RT-PCR (data not shown). Measurements showed no failure of transmission up to 50-Hz stimulation frequency in the mutant. The degree of CMAP decrement at 10- (not shown), 30-, or 50-Hz stimulation frequency was similar in mutants and wild-type littermate controls (Figures 4I and 4J). In contrast, spontaneous miniature endplate potentials (mEPPs) were increased by 40% in frequency (Figure 4K) but were not altered in amplitude (Figure 4L) in the mutant compared to wild-type animals. In addition, stimulated (1 Hz) EPPs were increased in amplitude secondary to an increased quantal content (QC), defined as the calculated number of acetylcholine-containing vesicles released per stimulation (Figures 4M and 4N). Labeling with antibodies to bassoon (Bssn), piccolo (Picc), two very large scaffolding proteins of the cytomatrix assembled at the active zone, and P/Q voltage-gated calcium channels (VGCCs) (Gundelfinger et al., 2016), showed no detectable differences in labeling intensity between *Chodl* mutants and wild-type mice (Figures S6F–S6N). This suggests that the number of available release sites is increased proportionally to the size of

Figure 4. *Chodl* Mutant Mice Show Morphological and Electrophysiological Synaptic Defects of the Neuromuscular Junction

(A and B) Representative confocal micrographs of two wild-type (A) and two *Chodl* mutant (B) neuromuscular junctions on hind limb lumbrical muscles from 4-month-old mice are shown. Neuronal tissue is labeled in green (2H3, neurofilament; SV2, synaptic vesicle protein 2), and post-synaptic AChRs are labeled in red (α-BTX, α-bungarotoxin).

(C and D) Both the pre-synaptic (C) and post-synaptic (D) areas are increased in *Chodl* mutant mice compared to wild-type mice (pre-synaptic area, *p = 0.0354; post-synaptic area, *p = 0.0176).

(E and F) The areas of synaptic contact (E) and endplate (F) are also increased in the *Chodl* mutant mice compared to wild-type mice (area of synaptic area, *p = 0.0158; endplate area, **p = 0.0062).

(G) *Chodl* mutant mice have more fragmented post-synaptic endplates compared to wild-type mice at 4 months of age (**p = 0.0047).

(H) No differences are detected in occupancy (overlap percentage) of post-synaptic elements in *Chodl* mutant compared to wild-type mice.

(I) There is no significant difference in the 30 Hz decrement of CMAP between wild-type and *Chodl* mutant mice.

(J) No significant difference was observed in the 50Hz decrement of CMAP between wild-type and *Chodl* mutant mice.

(K and L) mEPP frequency (K) but not amplitude (L) differs between *Chodl* mutant and wild-type mice (*p = 0.0242; statistical power = 0.6313).

(M and N) Quantal content (M) and EPP amplitude (N) differ between the groups (QC, **p = 0.0086; statistical power = 0.8138; EPP amplitude, **p = 0.0092; statistical power = 0.8044).

Each data point represents one animal. A total of 50–60 neuromuscular junctions are analyzed across 5 animals/genotype for (A)–(H). Data are represented as mean ± SEM. n.s., not significant. Scale bars, 30 μm.

See also Figures S5, S6, and S7.

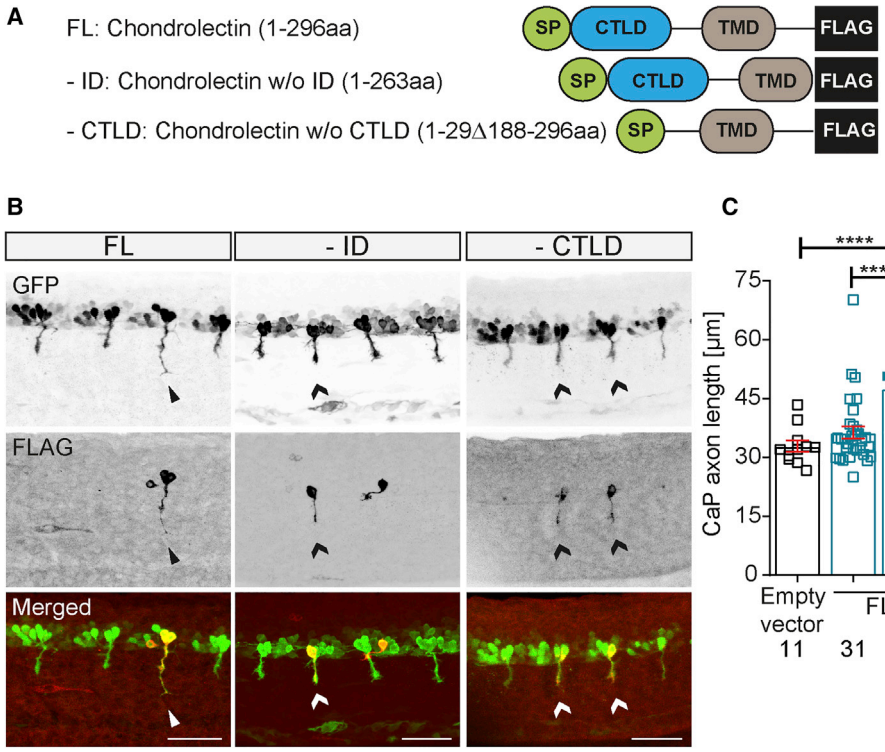

(legend on next page)

the enlarged synapse in *Chodl* mutants. However, we cannot exclude a contribution by increased calcium sensitivity of release sites to increased mEPP frequency and EPP amplitude/QC. Taken together, these data indicate altered neurotransmission at the neuromuscular junction in *Chodl* mutant mice.

Chodl Mutant Mice Show No Gross Alterations of Motor Behavior

Weights of *Chodl* mutant mice were not systematically different from wild-type controls at 2, 3, and 4 months of age (Figures S7A and S7B). An assessment of general locomotor activity in an open field environment revealed no differences in movement activity (light beam breaks in open field) and thigmotaxis (the tendency of mouse to remain close to the chamber lateral walls, a measurement for anxiety) in mutants, compared to wild-type animals (Figures S7C, S7D, and S7H). Motor coordination (accelerating rotarod test) and muscle strength (4-limb hanging wire test) did also not reveal any changes (Figures S7E–S7G). Although these tests did not detect changes in motor behavior in the *Chodl* mutant, more subtle alterations cannot be excluded.

C-Type Lectin Domain and Intracellular Domain Are Required to Mediate *chodl* Function

Because of the relative ease of phenotype analysis, we used the zebrafish to study the mechanistic basis of *chodl* function. The Chodl protein domain structure is typical of transmembrane recognition molecules, with an extracellular C-type lectin domain that may interact with extracellular binding partners, a transmembrane domain, and a short cytoplasmic tail with a number of potential phosphorylation sites that may be involved in intracellular signaling (Weng et al., 2002). To test for essential functions of different domains, we generated FLAG-tagged constructs missing either the C-type lectin domain or the intracellular domain for transient experimental expression in motor neurons of the *chodl* mutant, driven by the *mnx1* regulatory sequences (Figure 5A). Immuno-detection of the FLAG-tag indicated selective expression of constructs in motor neurons and their axons. All constructs reached the cell surface in transfected HEK293T cells (compare Figure 7A).

Only full-length Chodl showed rescuing activity in FLAG immuno-positive axons. FLAG-positive axons expressing full-length Chodl were 31% longer than FLAG-negative axons in the same embryos and 44.4% longer than axons in vector-injected embryos. Removing either the C-type lectin domain or intracellular domain resulted in no increase in axon length in FLAG immuno-positive axons compared to controls (Figures 5B and 5C).

To determine whether conformation and/or phosphorylation of the intracellular domain was essential, we mutated 10 of the 11 identified potential phosphorylation sites by replacing serine and threonine residues with alanine, leading to likely conformational changes and preventing phosphorylation of the intracellular domain (Figure 5D). This construct did not show rescuing activity of axon length, compared to the wild-type gene (Figures 5E and 5F). Hence, the C-type lectin domain and the intracellular domain of *chodl* are functionally important.

chodl and *col19a1* Show Genetic Interactions

The C-type lectin domain is likely to bind extracellular matrix (ECM) components, which are concentrated at the horizontal myoseptum (Schweitzer et al., 2005; Zhang et al., 2004), where axons stall in zebrafish *chodl* mutants. Mutants in the muscle-expressed *col19a1* (zebrafish mutant name: *stumpy*) show axon stalling at the horizontal myoseptum, as well as reduced axon branching and enlarged post-synaptic sites at the adult stage (Panzer et al., 2005). Because this phenotype is highly reminiscent of that of *chodl* mutants, we determined potential genetic interactions between *chodl* and *col19a1*. Using established (Hilario et al., 2010; Zhong et al., 2012) morpholinos, we found that injection of low concentrations of either morpholino alone elicited no or only weak changes of motor axon growth (Figures 6A and 6B). However, combining these morpholinos at the same concentrations led to synergistic effects on stalling of axons at the horizontal myoseptum. Of note, total morpholino load was kept at the same level for all experiments by adding non-specific control morpholino where appropriate. This indicates a genetic interaction between *chodl* and *col19a1* (Figures 6C and 6D).

Chodl Is a Specific Binding Partner for ColXIXa1

To determine a potential physical interaction of Chodl and ColXIXa1 proteins, we used co-immunoprecipitation. We tagged Chodl with a FLAG tag at its C-terminal end (Chodl-FLAG). ColXIXa1 was labeled with a hemagglutinin (HA) tag on either the N-terminal (HA-ColXIXa1) or the C-terminal end (ColXIXa1-HA) to control for possible interference of the tag with multimerization of the large protein (Figure 6E). Chodl-FLAG, purified from transfected HEK293T cells, was incubated with the supernatant of HA-ColXIXa1 and ColXIXa1-HA secreting HEK293T cells. An immunoprecipitation assay shows that Chodl-FLAG co-immunoprecipitated both HA-ColXIXa1 and ColXIXa1-HA (Figure 6F). Conversely, purified HA-ColXIXa1 and ColXIXa1-HA both pulled down Chodl-FLAG from cell lysates, indicating binding of the two proteins (Figure 6G).

Figure 5. C-Type Lectin Domain and Intracellular Domain Are Indispensable for Chodl Function.

(A) A cartoon indicating the constructs used in (B) is shown.

(B) Photomicrographs show representative images of mosaic construct expression in motor axons of *chodl* mutant zebrafish, detected by FLAG immunohistochemistry (lateral trunk views): full-length (FL), *chodl* without the C-type lectin (without [w/o] CTLD), or intracellular domains (w/o intracellular domain [ID]), are shown.

(C) Only injection of the full-length *chodl* construct partially rescues axon length in $FLAG^+$ motor axons (****$p < 0.0001$).

(D) A cartoon indicating the potential phosphorylation sites of the intracellular domain that are mutated to alanine (with [w/] ID S/T → A) is shown.

(E) Lateral trunk views of mutant *chodl* zebrafish expressing full-length *chodl* and mutated *chodl* are shown.

(F) Experimental expression of wild-type, but not mutated *chodl* in motor neurons partially rescues axonal length (****$p < 0.0001$; **$p = 0.001$).

Scale bars, 50 μm. Each data point represents one animal; data are represented as mean ± SEM; n.s., not significant; CTLD, C-type lectin domain.

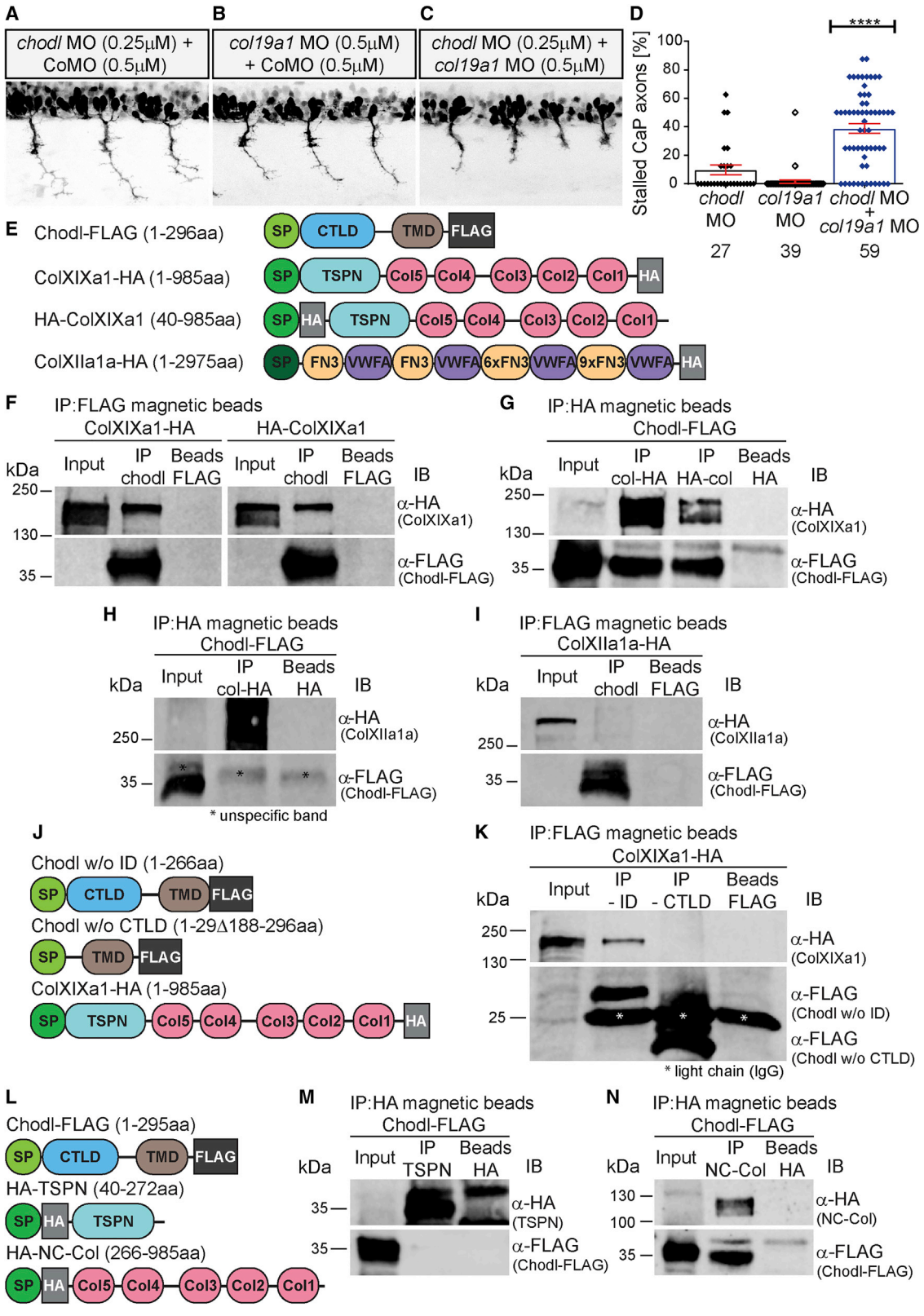

(legend on next page)

As a control, we used ColXIIa1a in co-immunoprecipitation experiments. Both ColXIIa1a and ColXIXa1 are Fibril-Associated Collagens with Interrupted Triple Helices (FACIT) family collagens (Bader et al., 2009; Hilario et al., 2010). ColXIIa1a is expressed in connective tissue and diffusely present at the nascent horizontal myoseptum at 24 hpf (Bader et al., 2009). Purified ColXIIa1a-HA did not pull down Chodl-FLAG from cell lysates of Chodl-FLAG overexpressing cells (Figure 6H), and purified Chodl-FLAG did not pull down ColXIIa1a from the supernatant of ColXIIa1a-HA transfected cells (Figure 6I). This indicates selective physical binding of Chodl to ColXIXa1.

To determine the Chodl domains necessary for ColXIXa1 binding, we used truncated versions of Chodl, with either the intracellular domain or the C-type lectin domain missing, for co-immunoprecipitation of full-length ColXIXa1-HA from supernatant (Figure 6J). Chodl without the intracellular domain, but not the version missing the C-type lectin domain, was still able to co-immunoprecipitate ColXIXa1-HA (Figure 6K). Conversely, using truncated versions of ColXIXa1, containing only the collagenous domains or only the thrombospondin domain (Figures 6L), we showed that only the truncated protein with the collagenous domains was able to co-immunoprecipitate Chodl-FLAG from lysates of overexpressing cells (Figures 6M and 6N). This supports a scenario in which the trans-membrane protein Chodl binds the collagenous repeats of ColXIXa1 at the cell surface by its extracellular C-type lectin domain.

Chodl Binds ColXIXa1 at the Cell Surface

To observe interactions of native Chodl and ColXIXa1 in intact cells, we incubated HEK293T cells that overexpress Chodl-FLAG with culture media containing ColXIXa1-HA for 24 h. Measuring immuno-fluorescence intensity across optical sections through fixed cells showed highest Chodl-FLAG immunoreactivity at the cells' edges (Figures 7A and 7B), consistent with trans-membrane localization. ColXIXa1-HA immunoreactivity on the cells was strong and located at the cell surface (Figures 7A and 7B). Incubating Chodl-FLAG overexpressing cells with ColXIIa1a-HA as a control showed only minimal fluorescence that did not coincide with Chodl-FLAG at the cell surface (Figures 7A and 7B). Likewise, cells transfected with membrane-bound EGFP as a control did not bind ColXIXa1-HA from the medium (Figures 7A and 7B). Expression of a construct missing the intracellular domain of Chodl still bound ColXIXa1 at the plasma membrane (Figures 7A and 7B). In contrast, the construct missing the C-type lectin domain of Chodl, which was still targeted to the membrane, did not localize ColXIXa1 from the supernatant to the cell membrane (Figures 7A and 7B). This indicates that native Chodl is a transmembrane protein that binds extracellular ColXIXa1 with its C-type lectin domain.

In the absence of specific antibodies to Chodl and ColXIXa1, it is not possible to determine whether the proteins co-localize *in vivo*. However, in the zebrafish rescue line (*chodl−/−; mnx1:chodl-FLAG*), in which axons deficient in endogenous *chodl* grow beyond the horizontal myoseptum with the support of experimentally expressed *chodl*, we observed the Chodl-FLAG protein in a punctate pattern along the axon, in close apposition with $AChR^{+}$ post-synaptic clusters (Figure 7C). This is consistent with a pre-synaptic function of Chodl.

In summary, our results indicate that Chodl on motor axons mediates essential interactions with ColXIXa1 in the muscle ECM. Without these interactions, synapses fail to form correctly and synapse-dependent axon growth and branching, as well as motor behaviors, are impaired (graphically summarized in Figure 7D).

DISCUSSION

Chodl Acts Primarily in Synaptogenesis

The increase in synaptic area at the horizontal myoseptum in zebrafish and lumbrical muscle of mouse *Chodl* mutants indicates an evolutionarily conserved role of the transmembrane molecule in synaptogenesis.

All observed *in vivo* phenotypes are potential consequences of defective synaptogenesis, supporting the notion of synapse-

Figure 6. *chodl* and *collagen19a1* Show Genetic Interaction and Protein Binding

(A–C) Sub-threshold application of both *chodl* (A; 0.25 μM) and *col19a1* (B; 0.5 μM) morpholinos (MOs) together with control morpholino (CoMO) do not induce aberrant motor axon growth. Combining the two active morpholinos at the same concentrations leads to axon stalling (C).

(D) Quantification of stalled axons (*chodl* morpholino + *col19a1* morpholino synergy versus hypothetical mean of *chodl* morpholino added to *col19a1* morpholino values, ****$p < 0.0001$). Each data point represents one animal; data are represented as mean ± SEM.

(E) Graphic presentations of the fusion proteins used in *in vitro* binding assays are shown. SP, signal peptide; CTLD, C-type lectin domain; TMD, transmembrane domain; FLAG, FLAG tag (DYKDDDDK); TSPN, thrombospondin N-terminal-like domain; Col, collagenous domain; HA, human influenza hemagglutinin tag; FN3, fibronectin type III domain; VWFA, von Willebrand factor type A domain.

(J) Graphic presentations of the fusion proteins used in *in vitro* binding assays are shown.

(L) A cartoon of the fusion proteins used in *in vitro* binding assays is shown.

(F) Purified FLAG-tagged chondrolectin binds HA-tagged CollagenXIXa1. As negative control, FLAG-empty magnetic beads are used. Number of independent experiments, n = 2 (HA-ColXIXa1, FLAG immunoprecipitation [IP]), n = 4 (ColXIXa1-HA, FLAG IP).

(G) HA-tagged CollagenXIXa1 interacts with FLAG-tagged chondrolectin. Empty HA-magnetic beads are used as negative controls. Number of independent experiments, n = 5 (Chodl-FLAG, HA IP).

(H) ColXIIa1 does not interact with FLAG-tagged Chodl. Number of independent experiments, m = 2.

(I) Purified chondrolectin does not pull down HA-tagged ColXIIa1. Empty HA-magnetic beads are used as negative controls. Number of independent expreiments, n = 2.

(K) FLAG-tagged chondrolectin without the intracellular domain (chodl w/o ID), but not without the C-type lectin domain (w/o CTLD), precipitates HA-tagged ColXIXa1 from culture media. Number of independent experiments, n = 4.

(M) The thrombospondin domain of ColXIXa1 (HA-TSPN) does not immuno-precipitates Chodl-FLAG. Number of independent experiments, n = 2 (HA-TSPN, HA IP).

(N) The collagenous repeats domain (HA-NC-Col) of ColXIXa1 immuno-precipitates Chodl-FLAG. Number of independent experiments, n = 4 (HA-NC-Col, HA IP).

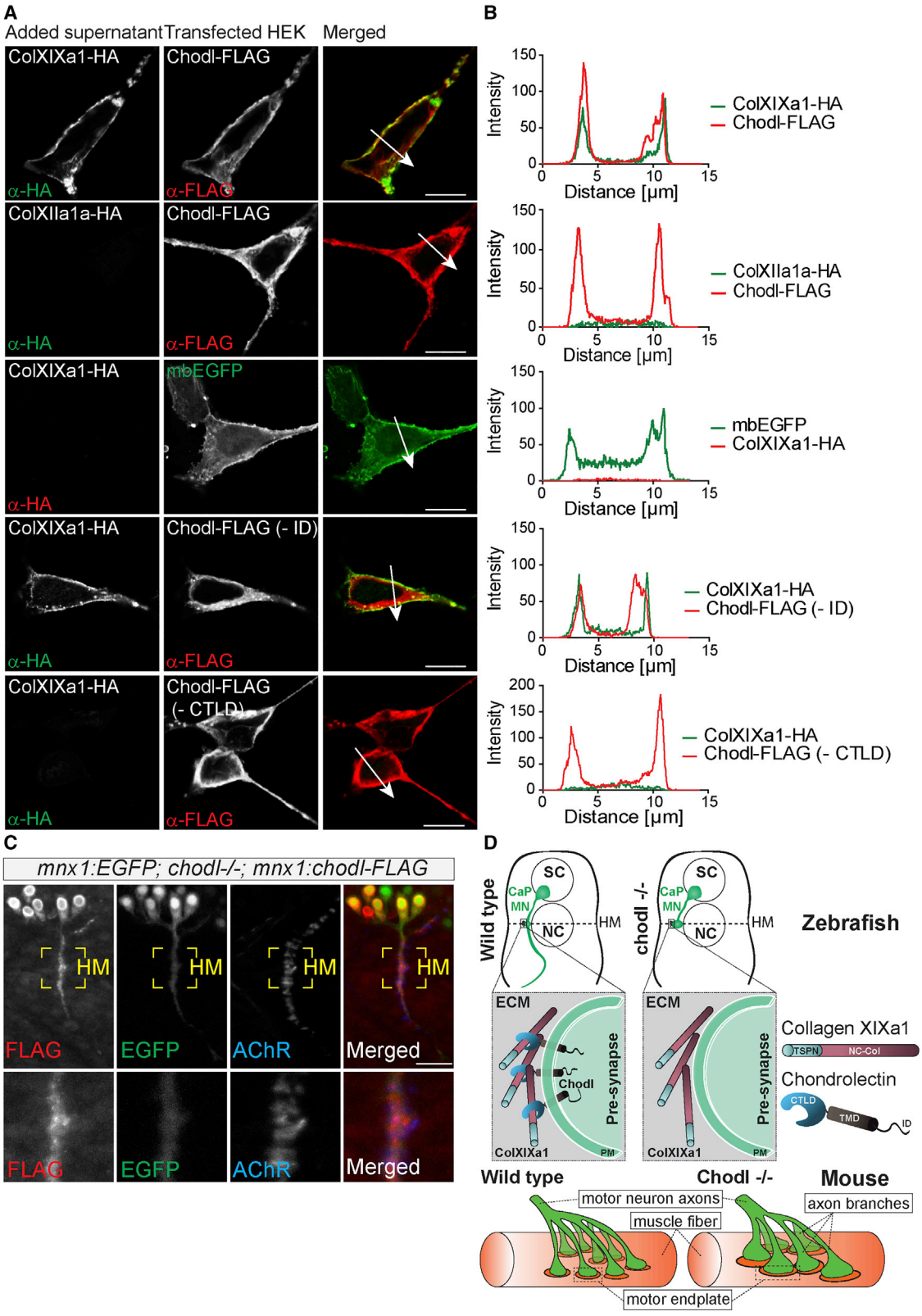

(legend on next page)

dependent motor axon growth in zebrafish. The phenotype of the CaP axon is prolonged stalling at the horizontal myoseptum. The horizontal myoseptum is a choice region in which the axons of the three primary motor neurons stall to integrate their pathway-specific cues (Beattie et al., 2002; Myers et al., 1986; Westerfield et al., 1986). However, the horizontal myoseptum is also a major synaptic site (Panzer et al., 2005; Panzer et al., 2006), and we show that in *chodl* mutants, synaptogenesis at this site is defective. Hence, formation of the nascent synapse might be a prerequisite for elongation of motor axons beyond the en passant synaptic site at the horizontal myoseptum. Indeed, naturally occurring pausing of CaP growth cones at the horizontal myoseptum might be due to the time required to form en passant synapses with muscle pioneers before growth can proceed (Eisen et al., 1986; Zhong et al., 2012), as in other systems (Hatada et al., 1999).

The idea that impaired synapse formation is what keeps the axon from growing in the *chodl* mutant is supported by our observation that filopodial dynamics is unperturbed. Filopodia extension has previously been identified as integral part of growth cone advance (Flanagan-Steet et al., 2005; Panzer et al., 2006). Moreover, in a previous time-lapse study, we have shown that when *chodl* expression is prevented, the speed of motor growth cone advance is unimpaired above and below the horizontal myoseptum site, suggesting that *chodl*-deficient axons are, in principle, capable of unimpaired growth (Zhong et al., 2012).

In 3-day-old mutant zebrafish, axon branching onto the muscle is strongly reduced. Motor axon branching has been suggested to depend on proper synaptogenesis in *Xenopus* larvae (Javaherian and Cline, 2005), in which new branches of motor axons always originate at a synaptic site. Our analysis of the branching pattern of motor axons in zebrafish larvae also shows that almost all axon branches onto the musculature occur at synapses. Synapse-dependent axon branching is also observed in the optic projection of *Xenopus* (Alsina et al., 2001) and zebrafish (Meyer and Smith, 2006), as well as in the thalamocortical projection in mammals (Matsumoto et al., 2016).

Mouse motor axons, which do not form en passant synapses during growth or branching at synaptic sites but mainly form terminal synapses instead (Sanes and Lichtman, 1999), did not show any obvious signs of reduced axon growth or branching in *Chodl* mutants. Hence, a lack of Chodl only affects synaptogenesis *in vivo*. However, *in vitro*, motor axons of *Chodl* mutant mice show reduced neurite growth, revealing a potential contribution of *Chodl* to axon growth that is compensated for *in vivo*.

The behavioral phenotype in zebrafish *chodl* mutants (reduced turn angle in escape response) is a likely consequence of hypo-innervation of the muscle tissue due to impaired synapse-dependent motor axon branching. In mice, we could not detect changes in CMAP or behavioral consequences of *Chodl* deficiency. However, the presence of anatomical and physiological phenotypes in *Chodl* mutant mice suggests that more sensitive tests might reveal deficits. Taken together, the above observations suggest an essential function of *Chodl* at the neuromuscular junction. Interestingly, *Chodl*- (Zeng and Sanes, 2017) and *Col19a1*-expressing neurons also exist in the cortex, and *Col19a1* mutant mice show synaptic defects (Su et al., 2016). This opens the perspective of more widespread roles of this ligand/receptor pair in synaptogenesis in other CNS regions.

ColXIXa1 Is a Binding Partner for Chodl

Immuno-precipitations show that the C-type lectin domain of Chodl binds the collagenous domains of ColXIXa1 but does not bind ColXIIa1a. However, other collagens could also act as a ligand, such as ColXV, which possesses collagenous domains (Eklund et al., 2000) and for which the mutant phenotype is also similar to that of *chodl* mutants in zebrafish (Guillon et al., 2016). Cell transfection assays indicate that binding of extracellular ColXIXa1 by the extracellular C-type lectin domains of Chodl occurs at the plasma membrane. This is consistent with known roles of the C-type lectin domain in recognition proteins of immune cells (Chiffoleau, 2018).

The horizontal myoseptum in zebrafish is rich in ECM factors, such as Tenascin-C (Schweitzer et al., 2005), Chondroitin sulfates (Zhang et al., 2004), and collagens (Guillon et al., 2016), which are likely to take part in synaptogenesis. The fact that ColXIXa1 is produced by muscle cells (Hilario et al., 2010) and Chodl by motor neurons (Zhong et al., 2012) makes it probable that these factors interact at the horizontal myoseptum synapses. This is supported by the observation that the *col19a1* mutant phenotype also entails prolonged stalling in this exact location (Beattie et al., 2000) and that knocking down *col19a1* and *chodl* leads to a synergistic increase in stalling specifically at the horizontal myoseptum, as we show here. Moreover, in functional rescue experiments, we find tagged Chodl along the motor axons, including the horizontal myoseptum region, indicating that functional Chodl is present at the horizontal myoseptum in motor axons. Specific antibodies to ColXIXa1 and Chodl, which are currently unavailable, would be needed to directly show interactions of endogenous proteins *in vivo*.

Figure 7. Experimentally Expressed Chodl Binds Extracellular ColXIXa1 at the Cell Surface and Is Targeted to Motor Axons.

(A and B) In transfected HEK cells, full-length constructs (Chodl-FLAG) and those without intracellular domain (Chodl-FLAG – ID) or C-type lectin domain (Chodl-FLAG – CTLD) show high plasma membrane labeling. Chodl-FLAG and Chodl-FLAG – ID bind ColXIXa1, but not ColXIIa1 (control), from supernatant at the cell surface. Cells transfected with membrane-bound EGFP (control) did not bind ColXIXa1. Single optical sections are shown in (A) and arrows indicate the measurement trajectories used to generate intensity profiles in (B). Number of individual experiments, 2.

(C) A lateral view of a motor axon that has grown beyond the horizontal myoseptum (HM) in a (*mnx1*:EGFP; *chodl*−/−; *mnx1*:chodl-FLAG) zebrafish embryo at 28 hpf is shown. Experimentally expressed Chodl-FLAG is present in the cytoplasm and punctate clusters along the axon (EGFP), overlaying the synapse area (AChR immunohistochemistry) at the horizontal myoseptum.

(D) Schematic summary of results is shown. Axonal *Chodl* is necessary to restrict the size of the neuromuscular junction by binding extracellular ColXIXa1. SC, spinal cord; CaP MN, caudal primary neuron; NC, notochord; HM, horizontal myoseptum; TSPN, thrombospondin domain; NC-Col, collagenous repeats; CTLD, C-type lectin domain; TMD, transmembrane domain.

Scale bar in (C): 20 μm; scale bars in (A): 10 μm.

Functional rescue experiments show that both the C-type lectin domain and intracellular domain are essential for Chodl function *in vivo*. Overall, this suggest a scenario in which axonal Chodl needs to bind muscle-derived ColXIXa1 to form proper synapses with muscle pioneers. ColXIXa1 binding likely leads to signaling events. This may involve binding of the intracellular domain to other proteins and/or changes in phosphorylation of the intracellular domain. The Chodl intracellular domain interacts with the Rab geranylgeranyl transferase β subunit *in vitro* (Claessens et al., 2008), but there are likely more interactions.

Connection of Chodl to SMA

Synapse destabilization is an early event in SMA disease progression (McGovern et al., 2008), and *Chodl* is dysregulated early in a mouse model of SMA (Bäumer et al., 2009; Zhang et al., 2008). With its role in synaptic development, dysregulation of *Chodl* may contribute to synaptic phenotypes in the disease. Indeed, overexpression of *chodl* partially rescues CaP axon growth defects in an SMA model in zebrafish (Sleigh et al., 2014a), supporting the hypothesis that dysregulation of *chodl* may be one of the disease mechanisms.

Of note, the rescue was only partial, and aberrations in CaP axon growth are more severe in SMA models than those seen in the *chodl* mutant here (Hao et al., 2013; McWhorter et al., 2003). Moreover, mouse SMA models show synaptic degeneration and motor neuron loss (Groen et al., 2018; Wishart et al., 2010), which we did not observe for the mouse *Chodl* mutant. It is, therefore, likely that dysregulation of other proteins in addition to *chodl* causes the phenotype in SMA models and the disease. Nevertheless, a lack of *chodl* replicates some synaptic defects seen in SMA models in zebrafish (Boon et al., 2009) and mice (Mentis et al., 2011), supporting that its dysregulation contributes to the disease phenotype. Interestingly, aberrant *chodl* expression has also been observed in a mouse ALS model (Wootz et al., 2010), and higher tissue levels of its binding partner COL19A1 are associated with faster disease progression in patients (Calvo et al., 2019).

Why is aberrant growth of motor axons in zebrafish a sensitive indicator of SMA- (Giacomotto et al., 2015; Oprea et al., 2008) and ALS- (Kabashi et al., 2011; Van Hoecke et al., 2012) related manipulations *in vivo*? In mouse models of motor neuron diseases, aberrant axon growth is rare, but aberrations of synapse formation are observed, as well as a later loss of motor neurons (McGovern et al., 2008; Mentis et al., 2011). One possible explanation is that axon growth in zebrafish, but not mice, is synapse dependent. Hence, aberrant motor axon growth in zebrafish SMA and other motor neuron disease models (Thomas-Jinu et al., 2017) might be a consequence of impaired expression of genes involved in synaptogenesis or synapse stabilization, such as *chodl*. However, other affected cellular mechanisms (Boyd et al., 2017; Donlin-Asp et al., 2016; Groen and Gillingwater, 2015) may also cause axonal aberrations in zebrafish.

In conclusion, we describe a new ligand receptor interaction between the survival motor neuron (SMN) downstream gene *Chodl* and *ColXIXa1* that is necessary for the formation of neuromuscular junctions and subsequent motor axon growth and branching in zebrafish.

STAR★METHODS

Detailed methods are provided in the online version of this paper and include the following:

- KEY RESOURCES TABLE
- LEAD CONTACT AND MATERIALS AVAILABILITY
- EXPERIMENTAL MODEL AND SUBJECT DETAILS
  - Zebrafish
  - Mouse
  - Cell culture
- METHOD DETAILS
  - Plasmids for zebrafish
  - Generation of a chodl mutant zebrafish
  - Generation of trasngenic zebrafish line
  - Zebrafish DNA extraction and genotyping
  - Zebrafish qRT-PCR
  - Double-morpholino injections in zebrafish
  - Acute rescue assays of motor axon length in zebrafish
  - Zebrafish whole-mount immunohistochemistry
  - Zebrafish phalloidin staining and analysis
  - Zebrafish whole-mount confocal imaging
  - Synaptic puncta quantification in zebrafish
  - Time-lapse imaging of axon filopodia in zebrafish
  - Analysis of MiP motor axons in zebrafish
  - Zebrafish larval behavior analysis
  - Genotyping PCR for mice
  - Mouse primary motor neuron cell culture
  - *Ex vivo* electrophysiology in mice
  - Mouse muscle preparation and immunohistochemistry
  - Behavioral analysis in mice
  - HEK293T transfection and binding assays
  - Immuno-labeling of transfected HEK293T cells
  - Protein binding assays
- QUANTIFICATION AND STATISTICAL ANALYSIS
- DATA AND CODE AVAILABILITY

SUPPLEMENTAL INFORMATION

Supplemental Information can be found online at https://doi.org/10.1016/j.celrep.2019.09.033.

ACKNOWLEDGMENTS

We thank Prof. Thomas Gillingwater for advice on histological analysis of the neuromuscular junction. The C57BL/6NTac-Chodl$^{em1(IMPC)H}$/H mice were obtained from the MRC Harwell Institute, which distributes these mice on behalf of the European Mouse Mutant Archive (https://www.infrafrontier.eu/). The MRC Harwell Institute is a member of the International Mouse Phenotyping Consortium (IMPC) and received funding from the Medical Research Council for generating and phenotyping the C57BL/6NTac-Chodl$^{em1(IMPC)H}$/H mice. The research reported in this publication is solely the responsibility of the authors and does not necessarily represent the official views of the Medical Research Council. Funding details and associated primary phenotypic information may be found at https://www.mousephenotype.org. K.T. and C.G.B. are part of the UK SMA Research Consortium funded by the SMA Trust. H.L.S. was funded by an MND Association PhD studentship (871-792), M.J.C. by an EMBO Long-Term Fellowship (ALTF 946-2014), and D.W. by a Fellowship of the Deutsche Forschungsgemeinschaft (WE5736/1-1).

AUTHOR CONTRIBUTIONS

Conceptualization, T.B., K.T., and C.G.B.; Methodology, A.-M.O., H.L.S., and S.A.; Investigation, A.-M.O., H.L.S., S.A., R.W., Z.Z., D.W., and M.J.C.; Writing – Original Draft, T.B., K.T., and C.G.B.; Writing – Review & Editing, T.B., K.T., and C.G.B.; Funding Acquisition, K.T. and C.G.B.; Supervision, T.B., K.T., and C.G.B.

DECLARATION OF INTERESTS

The authors declare no competing interests.

Received: May 6, 2019
Revised: August 13, 2019
Accepted: September 12, 2019
Published: October 29, 2019

REFERENCES

Alsina, B., Vu, T., and Cohen-Cory, S. (2001). Visualizing synapse formation in arborizing optic axons in vivo: dynamics and modulation by BDNF. Nat. Neurosci. *4*, 1093–1101.

Anderson, J.L., Mulligan, T.S., Shen, M.C., Wang, H., Scahill, C.M., Tan, F.J., Du, S.J., Busch-Nentwich, E.M., and Farber, S.A. (2017). mRNA processing in mutant zebrafish lines generated by chemical and CRISPR-mediated mutagenesis produces unexpected transcripts that escape nonsense-mediated decay. PLoS Genet. *13*, e1007105.

Aydin, H., Azimi, F.C., Cook, J.D., and Lee, J.E. (2012). A convenient and general expression platform for the production of secreted proteins from human cells. J. Vis. Exp., 4041.

Bader, H.L., Keene, D.R., Charvet, B., Veit, G., Driever, W., Koch, M., and Ruggiero, F. (2009). Zebrafish collagen XII is present in embryonic connective tissue sheaths (fascia) and basement membranes. Matrix Biol. *28*, 32–43.

Balciunas, D., Wangensteen, K.J., Wilber, A., Bell, J., Geurts, A., Sivasubbu, S., Wang, X., Hackett, P.B., Largaespada, D.A., McIvor, R.S., and Ekker, S.C. (2006). Harnessing a high cargo-capacity transposon for genetic applications in vertebrates. PLoS Genet. *2*, e169.

Bäumer, D., Lee, S., Nicholson, G., Davies, J.L., Parkinson, N.J., Murray, L.M., Gillingwater, T.H., Ansorge, O., Davies, K.E., and Talbot, K. (2009). Alternative splicing events are a late feature of pathology in a mouse model of spinal muscular atrophy. PLoS Genet. *5*, e1000773.

Beattie, C.E., Melancon, E., and Eisen, J.S. (2000). Mutations in the stumpy gene reveal intermediate targets for zebrafish motor axons. Development *127*, 2653–2662.

Beattie, C.E., Granato, M., and Kuwada, J.Y. (2002). Cellular, genetic and molecular mechanisms of axonal guidance in the zebrafish. Results Probl. Cell Differ. *40*, 252–269.

Boon, K.L., Xiao, S., McWhorter, M.L., Donn, T., Wolf-Saxon, E., Bohnsack, M.T., Moens, C.B., and Beattie, C.E. (2009). Zebrafish survival motor neuron mutants exhibit presynaptic neuromuscular junction defects. Hum. Mol. Genet. *18*, 3615–3625.

Boyd, P.J., Tu, W.Y., Shorrock, H.K., Groen, E.J.N., Carter, R.N., Powis, R.A., Thomson, S.R., Thomson, D., Graham, L.C., Motyl, A.A.L., et al. (2017). Bioenergetic status modulates motor neuron vulnerability and pathogenesis in a zebrafish model of spinal muscular atrophy. PLoS Genet. *13*, e1006744.

Calvo, A.C., Cibreiro, G.A., Merino, P.T., Roy, J.F., Galiana, A., Rufián, A.J., Cano, J.M., Martín, M.A., Moreno, L., Larrodé, P., et al. (2019). Collagen XIX Alpha 1 Improves Prognosis in Amyotrophic Lateral Sclerosis. Aging Dis. *10*, 278–292.

Chiffoleau, E. (2018). C-Type Lectin-Like Receptors As Emerging Orchestrators of Sterile Inflammation Represent Potential Therapeutic Targets. Front. Immunol. *9*, 227.

Claessens, A., Weyn, C., and Merregaert, J. (2008). The cytoplasmic domain of chondrolectin interacts with the beta-subunit of Rab geranylgeranyl transferase. Cell. Mol. Biol. Lett. *13*, 250–259.

Devoto, S.H., Melançon, E., Eisen, J.S., and Westerfield, M. (1996). Identification of separate slow and fast muscle precursor cells in vivo, prior to somite formation. Development *122*, 3371–3380.

Donlin-Asp, P.G., Bassell, G.J., and Rossoll, W. (2016). A role for the survival of motor neuron protein in mRNP assembly and transport. Curr. Opin. Neurobiol. *39*, 53–61.

Eisen, J.S., Myers, P.Z., and Westerfield, M. (1986). Pathway selection by growth cones of identified motoneurones in live zebra fish embryos. Nature *320*, 269–271.

Eklund, L., Muona, A., Liétard, J., and Pihlajaniemi, T. (2000). Structure of the mouse type XV collagen gene, Col15a1, comparison with the human COL15A1 gene and functional analysis of the promoters of both genes. Matrix Biol. *19*, 489–500.

Enjin, A., Rabe, N., Nakanishi, S.T., Vallstedt, A., Gezelius, H., Memic, F., Lind, M., Hjalt, T., Tourtellotte, W.G., Bruder, C., et al. (2010). Identification of novel spinal cholinergic genetic subtypes disclose Chodl and Pitx2 as markers for fast motor neurons and partition cells. J. Comp. Neurol. *518*, 2284–2304.

Faul, F., Erdfelder, E., Buchner, A., and Lang, A.G. (2009). Statistical power analyses using G*Power 3.1: tests for correlation and regression analyses. Behav. Res. Methods *41*, 1149–1160.

Flanagan-Steet, H., Fox, M.A., Meyer, D., and Sanes, J.R. (2005). Neuromuscular synapses can form in vivo by incorporation of initially aneural postsynaptic specializations. Development *132*, 4471–4481.

Giacomotto, J., Rinkwitz, S., and Becker, T.S. (2015). Effective heritable gene knockdown in zebrafish using synthetic microRNAs. Nat. Commun. *6*, 7378.

Groen, E.J.N., and Gillingwater, T.H. (2015). UBA1: At the Crossroads of Ubiquitin Homeostasis and Neurodegeneration. Trends Mol. Med. *21*, 622–632.

Groen, E.J.N., Perenthaler, E., Courtney, N.L., Jordan, C.Y., Shorrock, H.K., van der Hoorn, D., Huang, Y.T., Murray, L.M., Viero, G., and Gillingwater, T.H. (2018). Temporal and tissue-specific variability of SMN protein levels in mouse models of spinal muscular atrophy. Hum. Mol. Genet. *27*, 2851–2862.

Guillon, E., Bretaud, S., and Ruggiero, F. (2016). Slow Muscle Precursors Lay Down a Collagen XV Matrix Fingerprint to Guide Motor Axon Navigation. J. Neurosci. *36*, 2663–2676.

Gundelfinger, E.D., Reissner, C., and Garner, C.C. (2016). Role of Bassoon and Piccolo in Assembly and Molecular Organization of the Active Zone. Front. Synaptic Neurosci. *7*, 19.

Hao, T., Duy, P.Q., Jontes, J.D., Wolman, M., Granato, M., and Beattie, C.E. (2013). Temporal requirement for SMN in motoneuron development. Hum. Mol. Genet. *22*, 2612–2625.

Hatada, Y., Wu, F., Silverman, R., Schacher, S., and Goldberg, D.J. (1999). En passant synaptic varicosities form directly from growth cones by transient cessation of growth cone advance but not of actin-based motility. J. Neurobiol. *41*, 242–251.

Hilario, J.D., Wang, C., and Beattie, C.E. (2010). Collagen XIXa1 is crucial for motor axon navigation at intermediate targets. Development *137*, 4261–4269.

Jao, L.E., Wente, S.R., and Chen, W. (2013). Efficient multiplex biallelic zebrafish genome editing using a CRISPR nuclease system. Proc. Natl. Acad. Sci. USA *110*, 13904–13909.

Javaherian, A., and Cline, H.T. (2005). Coordinated motor neuron axon growth and neuromuscular synaptogenesis are promoted by CPG15 *in vivo*. Neuron *45*, 505–512.

Jones, R.A., Reich, C.D., Dissanayake, K.N., Kristmundsdottir, F., Findlater, G.S., Ribchester, R.R., Simmen, M.W., and Gillingwater, T.H. (2016). NMJ-morph reveals principal components of synaptic morphology influencing structure-function relationships at the neuromuscular junction. Open Biol. *6*, 160240.

Kabashi, E., Bercier, V., Lissouba, A., Liao, M., Brustein, E., Rouleau, G.A., and Drapeau, P. (2011). FUS and TARDBP but not SOD1 interact in genetic models of amyotrophic lateral sclerosis. PLoS Genet. *7*, e1002214.

Korzh, S., Winata, C.L., Zheng, W., Yang, S., Yin, A., Ingham, P., Korzh, V., and Gong, Z. (2011). The interaction of epithelial Ihha and mesenchymal Fgf10 in zebrafish esophageal and swimbladder development. Dev. Biol. *359*, 262–276.

Kwon, M., and Firestein, B.L. (2013). DNA transfection: calcium phosphate method. Methods Mol. Biol. *1018*, 107–110.

Martínez-Silva, M.L., Imhoff-Manuel, R.D., Sharma, A., Heckman, C.J., Shneider, N.A., Roselli, F., Zytnicki, D., and Manuel, M. (2018). Hypoexcitability precedes denervation in the large fast-contracting motor units in two unrelated mouse models of ALS. eLife *7*, e30955.

Matsumoto, N., Hoshiko, M., Sugo, N., Fukazawa, Y., and Yamamoto, N. (2016). Synapse-dependent and independent mechanisms of thalamocortical axon branching are regulated by neuronal activity. Dev. Neurobiol. *76*, 323–336.

McGovern, V.L., Gavrilina, T.O., Beattie, C.E., and Burghes, A.H. (2008). Embryonic motor axon development in the severe SMA mouse. Hum. Mol. Genet. *17*, 2900–2909.

McWhorter, M.L., Monani, U.R., Burghes, A.H., and Beattie, C.E. (2003). Knockdown of the survival motor neuron (Smn) protein in zebrafish causes defects in motor axon outgrowth and pathfinding. J. Cell Biol. *162*, 919–931.

Melançon, E., Liu, D.W., Westerfield, M., and Eisen, J.S. (1997). Pathfinding by identified zebrafish motoneurons in the absence of muscle pioneers. J. Neurosci. *17*, 7796–7804.

Mentis, G.Z., Blivis, D., Liu, W., Drobac, E., Crowder, M.E., Kong, L., Alvarez, F.J., Sumner, C.J., and O'Donovan, M.J. (2011). Early functional impairment of sensory-motor connectivity in a mouse model of spinal muscular atrophy. Neuron *69*, 453–467.

Meyer, M.P., and Smith, S.J. (2006). Evidence from in vivo imaging that synaptogenesis guides the growth and branching of axonal arbors by two distinct mechanisms. J. Neurosci. *26*, 3604–3614.

Myers, P.Z., Eisen, J.S., and Westerfield, M. (1986). Development and axonal outgrowth of identified motoneurons in the zebrafish. J. Neurosci. *6*, 2278–2289.

Oprea, G.E., Kröber, S., McWhorter, M.L., Rossoll, W., Müller, S., Krawczak, M., Bassell, G.J., Beattie, C.E., and Wirth, B. (2008). Plastin 3 is a protective modifier of autosomal recessive spinal muscular atrophy. Science *320*, 524–527.

Panzer, J.A., Gibbs, S.M., Dosch, R., Wagner, D., Mullins, M.C., Granato, M., and Balice-Gordon, R.J. (2005). Neuromuscular synaptogenesis in wild-type and mutant zebrafish. Dev. Biol. *285*, 340–357.

Panzer, J.A., Song, Y., and Balice-Gordon, R.J. (2006). In vivo imaging of preferential motor axon outgrowth to and synaptogenesis at prepatterned acetylcholine receptor clusters in embryonic zebrafish skeletal muscle. J. Neurosci. *26*, 934–947.

Ran, F.A., Hsu, P.D., Wright, J., Agarwala, V., Scott, D.A., and Zhang, F. (2013). Genome engineering using the CRISPR-Cas9 system. Nat. Protoc. *8*, 2281–2308.

Riedl, J., Crevenna, A.H., Kessenbrock, K., Yu, J.H., Neukirchen, D., Bista, M., Bradke, F., Jenne, D., Holak, T.A., Werb, Z., et al. (2008). Lifeact: a versatile marker to visualize F-actin. Nat. Methods *5*, 605–607.

Rishal, I., Golani, O., Rajman, M., Costa, B., Ben-Yaakov, K., Schoenmann, Z., Yaron, A., Basri, R., Fainzilber, M., and Galun, M. (2013). WIS-NeuroMath enables versatile high throughput analyses of neuronal processes. Dev. Neurobiol. *73*, 247–256.

Sanes, J.R., and Lichtman, J.W. (1999). Development of the vertebrate neuromuscular junction. Annu. Rev. Neurosci. *22*, 389–442.

Schneider, C.A., Rasband, W.S., and Eliceiri, K.W. (2012). NIH Image to ImageJ: 25 years of image analysis. Nat. Methods *9*, 671–675.

Schweitzer, J., Becker, T., Lefebvre, J., Granato, M., Schachner, M., and Becker, C.G. (2005). Tenascin-C is involved in motor axon outgrowth in the trunk of developing zebrafish. Dev. Dyn. *234*, 550–566.

Sleigh, J.N., Barreiro-Iglesias, A., Oliver, P.L., Biba, A., Becker, T., Davies, K.E., Becker, C.G., and Talbot, K. (2014a). Chondrolectin affects cell survival and neuronal outgrowth in in vitro and in vivo models of spinal muscular atrophy. Hum. Mol. Genet. *23*, 855–869.

Sleigh, J.N., Burgess, R.W., Gillingwater, T.H., and Cader, M.Z. (2014b). Morphological analysis of neuromuscular junction development and degeneration in rodent lumbrical muscles. J. Neurosci. Methods *227*, 159–165.

Su, J., Chen, J., Lippold, K., Monavarfeshani, A., Carrillo, G.L., Jenkins, R., and Fox, M.A. (2016). Collagen-derived matricryptins promote inhibitory nerve terminal formation in the developing neocortex. J. Cell Biol. *212*, 721–736.

Thomas-Jinu, S., Gordon, P.M., Fielding, T., Taylor, R., Smith, B.N., Snowden, V., Blanc, E., Vance, C., Topp, S., Wong, C.H., et al. (2017). Non-nuclear Pool of Splicing Factor SFPQ Regulates Axonal Transcripts Required for Normal Motor Development. Neuron *94*, 322–336.e5.

Van Hoecke, A., Schoonaert, L., Lemmens, R., Timmers, M., Staats, K.A., Laird, A.S., Peeters, E., Philips, T., Goris, A., Dubois, B., et al. (2012). EPHA4 is a disease modifier of amyotrophic lateral sclerosis in animal models and in humans. Nat. Med. *18*, 1418–1422.

Webster, R.G., Cossins, J., Lashley, D., Maxwell, S., Liu, W.W., Wickens, J.R., Martinez-Martinez, P., de Baets, M., and Beeson, D. (2013). A mouse model of the slow channel myasthenic syndrome: Neuromuscular physiology and effects of ephedrine treatment. Exp. Neurol. *248*, 286–298.

Wehner, D., Tsarouchas, T.M., Michael, A., Haase, C., Weidinger, G., Reimer, M.M., Becker, T., and Becker, C.G. (2017). Wnt signaling controls pro-regenerative Collagen XII in functional spinal cord regeneration in zebrafish. Nat. Commun. *8*, 126.

Wen, H., Linhoff, M.W., McGinley, M.J., Li, G.L., Corson, G.M., Mandel, G., and Brehm, P. (2010). Distinct roles for two synaptotagmin isoforms in synchronous and asynchronous transmitter release at zebrafish neuromuscular junction. Proc. Natl. Acad. Sci. USA *107*, 13906–13911.

Weng, L., Smits, P., Wauters, J., and Merregaert, J. (2002). Molecular cloning and characterization of human chondrolectin, a novel type I transmembrane protein homologous to C-type lectins. Genomics *80*, 62–70.

Westerfield, M. (2000). The Zebrafish Book: a Guide for the Laboratory Use of Zebrafish (*Danio rerio*), Fourth Edition (University of Oregon Press).

Westerfield, M., McMurray, J.V., and Eisen, J.S. (1986). Identified motoneurons and their innervation of axial muscles in the zebrafish. J. Neurosci. *6*, 2267–2277.

Wiese, S., Herrmann, T., Drepper, C., Jablonka, S., Funk, N., Klausmeyer, A., Rogers, M.L., Rush, R., and Sendtner, M. (2010). Isolation and enrichment of embryonic mouse motoneurons from the lumbar spinal cord of individual mouse embryos. Nat. Protoc. *5*, 31–38.

Wishart, T.M., Huang, J.P., Murray, L.M., Lamont, D.J., Mutsaers, C.A., Ross, J., Geldsetzer, P., Ansorge, O., Talbot, K., Parson, S.H., and Gillingwater, T.H. (2010). SMN deficiency disrupts brain development in a mouse model of severe spinal muscular atrophy. Hum. Mol. Genet. *19*, 4216–4228.

Wootz, H., Enjin, A., Wallén-Mackenzie, A., Lindholm, D., and Kullander, K. (2010). Reduced VGLUT2 expression increases motor neuron viability in Sod1(G93A) mice. Neurobiol. Dis. *37*, 58–66.

Zeng, H., and Sanes, J.R. (2017). Neuronal cell-type classification: challenges, opportunities and the path forward. Nat. Rev. Neurosci. *18*, 530–546.

Zhang, J., Lefebvre, J.L., Zhao, S., and Granato, M. (2004). Zebrafish unplugged reveals a role for muscle-specific kinase homologs in axonal pathway choice. Nat. Neurosci. *7*, 1303–1309.

Zhang, Z., Lotti, F., Dittmar, K., Younis, I., Wan, L., Kasim, M., and Dreyfuss, G. (2008). SMN deficiency causes tissue-specific perturbations in the repertoire of snRNAs and widespread defects in splicing. Cell *133*, 585–600.

Zhong, Z., Ohnmacht, J., Reimer, M.M., Bach, I., Becker, T., and Becker, C.G. (2012). Chondrolectin mediates growth cone interactions of motor axons with an intermediate target. J. Neurosci. *32*, 4426–4439.

STAR★METHODS

KEY RESOURCES TABLE

REAGENT or RESOURCE	SOURCE	IDENTIFIER
Antibodies		
Rabbit anti-Tuj1	Covance	N/A
Mouse anti-Islet1	DSHB	Cat# 40.2D6; RRID:AB_528315
Mouse anti- 2H3, neurofilament (NF-M)	DSHB	2H3; RRID:AB_531793
Mouse anti-bassoon, clone name- SAP7F407	BioScience, Nottingham	Cat# GTX13249; RRID:AB_422275
Rabbit anti-piccolo	Synaptic Systems, Germany	Cat# 142002; RRID:AB_887759
Rabbit anti-P/Q-VGCC (Cav2.1)	Synaptic Systems, Germany	Cat# 152203; RRID:AB_2619841
Anti-p75 NGF Receptor antibody [MLR2]	Abcam	Cat# ab61425; RRID:AB_943967
Chicken anti-GFP	Abcam	Cat# AB13970; RRID:AB_300798
Mouse anti- SV2, Synaptic vesicle glycoprotein 2A	DSHB	SV2; RRID:AB_2315387
Mouse anti-Znp-1	DSHB	Znp1; RRID:AB_531910
Rat anti-AChR	DSHB	mAb35; RRID:AB_528405
Rabbit anti-FLAG	Cell Signaling Technology	Cat# 14793; RRID:AB_2572291
Mouse anti-FLAG	Sigma-Aldrich	Cat# F1804; RRID:AB_262044
Mouse anti-HA	BioLegend	Cat# 901501; RRID:AB_2565006
Alexa Fluor 488 anti-phalloidin	ThermoFisher Scientific	Cat# A12380
Tetramethylrhodamine (TRITC) a-BTX- 568	Cambridge Bioscience	Cat# BT00012
Alexa Fluor ® 488 Donkey anti-mouse	ThermoFisher Scientific	Cat# A21202; RRID:AB_141607
Alexa Fluor ® 488 Donkey anti-rabbit	ThermoFisher Scientific	Cat# A21206; RRID:AB_2535792
Alexa Fluor ® 488 Goat-anti rabbit	ThermoFisher Scientific	Cat# A27034; RRID:AB_2536097
Alexa Fluor ® 568 Goat-anti rabbit	ThermoFisher Scientific	Cat# A11011; RRID:AB_143157
Alexa Fluor ® 488 Goat anti-mouse	ThermoFisher Scientific	Cat# A28175; RRID:AB_2536161
Alexa Fluor ® 488 AffiniPure Donkey Anti-Chicken IgY (IgG) (H+L)	Jackson ImmunoResearch	Cat# 703-545-155; RRID:AB_2340375
Alexa Fluor® 594 AffiniPure Donkey Anti-Mouse IgG (H+L)	Jackson ImmunoResearch	Cat# 715-585-150; RRID:AB_2340854
Alexa Fluor® 594 AffiniPure Donkey Anti-Mouse IgG (H+L) (Minimally cross-reactive to Rat, pre-adsorbed)	Jackson ImmunoResearch	Cat# 715-585-151; RRID:AB_2340855
Alexa Fluor® 488 AffiniPure Donkey Anti-Rat IgG (H+L) (minimally cross-reactive to Mouse, pre-adsorbed)	Jackson ImmunoResearch	Cat# 712-545-153; RRID:AB_2340684
Alexa Fluor® 647 AffiniPure Donkey Anti-Rat IgG (H+L) (Minimally cross-reactive to Mouse, pre-adsorbed)	Jackson ImmunoResearch	Cat# 712-605-153; RRID:AB_2340694
Alexa Fluor® 647 AffiniPure Donkey Anti-Rabbit IgG (H+L)	Jackson ImmunoResearch	Cat# 711-605-152; RRID:AB_2492288
Alexa Fluor® 488 AffiniPure Donkey Anti-Mouse IgG (H+L)	Jackson ImmunoResearch	Cat# 715-545-150; RRID:AB_2340846
Alexa Fluor® 647 AffiniPure Donkey Anti-Mouse IgG (H+L)	Jackson ImmunoResearch	Cat# 715-605-150; RRID:AB_2340862
IRDye 800CW Goat anti-Mouse IgG (H + L) Highly Cross-Adsorbed	Li-Cor	Cat# 925-32210; RRID:AB_2687825
IRDye 680LT Goat anti-Rabbit IgG (H + L) Highly Cross-Adsorbed	Li-Cor	Cat# 925-68021; RRID:AB_2713919
FLAG M2 magnetic beads	Sigma-Aldrich	Cat# M8823; RRID:AB_2637089
HA magnetic beads	ThermoFisher Scientific	Cat# 88836; RRID:AB_2749815

(*Continued on next page*)

Continued

REAGENT or RESOURCE	SOURCE	IDENTIFIER
Chemicals, Peptides, and Recombinant Proteins		
Poly-DL-ornithine hydrobromide	Sigma	Cat# P8638
Recombinant Human CNTF	Peprotech	Cat# 450-13
Recombinant Human/Murine/Rat BDNF	Peprotech	Cat# 450-02
Recombinant Human GDNF	Peprotech	Cat# 450-10
Recombinant Human NT-3	Peprotech	Cat# 450-03
u-Conotoxin GIIIB	Peptide Institute	Cat# 4217v
Poly-D-Lysine solution, 1.0 mg/ml	Merck Millipore Corporation	Cat# A-003-E
Critical Commercial Assays		
PureLink Genomic DNA Kit	Thermo Fisher Scientific	Cat# K182001
Lipofectamine 2000 Transfection Reagent	ThermoFisher Scientific	Cat# 11668030
mMessage mMachine T7 Transcription kit	ThermoFisher Scientific	Cat# AM1344
mirVana miRNA kit	ThermoFisher Scientific	Cat# AM1560
mMessage mMachine T3 Transcription kit	ThermoFisher Scientific	Cat# AM1348
RNeasy Mini Kit	QIAGEN	Cat# 74106
iScript cDNA Synthesis Kit	Bio-Rad	Cat# 170-8891
SsoAdvanced Universal SYBR Green Supermix	Bio-Rad	Cat# 1725271
Deposited Data		
File containing the original western blotting images	Mendeley Data	https://doi.org/10.17632/g23ts8jjpp.1
File containing the Coomassie gels	Mendeley Data	https://doi.org/10.17632/g23ts8jjpp.1
Experimental Models: Cell Lines		
HEK293T cells	Culture Collections Public Health England Porton Down, Salisbury, UK	N/A
Experimental Models: Organisms/Strains		
Chodl $^{em1(IMPC)H}$ - C57BL/6NTac background	https://www.mousephenotype.org/	https://www.infrafrontier.eu/
WIK wild type strain of zebrafish	European Zebrafish Resource Center (EZRC)	https://zfin.org/action/genotype/view/ZDB-GENO-010531-2
Tg (mnx1:GFP)	Flanagan-Steet et al., 2005	N/A
chodl −/−; mnx1:GFP	This paper	N/A
chodl−/−; mnx1:chodl-FLAG	This paper	N/A
Oligonucleotides		
Mouse Chodl genotyping Pair A, Forward:5′- AC GTGAGTTTAGAGGGAAAGTTTG −3′	This paper	N/A
Mouse Chodl genotyping Pair A, Reverse: 5′- CA GGATTGGCAGTTGGTTGGT −3′	This paper	N/A
Mouse Chodl genotyping Pair B, Forward: 5′-GGC TGGCTTGTGAAAGTGAAG-3′	This paper	N/A
Mouse Chodl genotyping Pair B, Reverse: 5′ -GTT TGGCCATCTCCGCTTCT-3′	This paper	N/A
Morpholino: MO-colXIXa1 GGCAAACCCTGCAAG CCAAAGGAG	GeneTool	N/A
gRNA targeting sequence zf *chodl* (exon 1) Forward: 5′ -TAGGAGGATGCGCGCGACACTC - 3′	This paper	N/A
gRNA targeting sequence zf *chodl* (exon 1) Reverse: 5′ - AAACGAGTGTCGCGCGCATCCT – 3′	This paper	N/A
Zf *chodl* genotyping Forward: 5′ – GACTGGAGCAA GTCTGTG – 3′	This paper	N/A
Zf *chodl* genotyping Reverse: 5′ – CTGCACGAGAC CAGAAAA – 3′	This paper	N/A
Primers for *chodl* mutagenesis, see Table S1	This paper	N/A

(*Continued on next page*)

Continued

REAGENT or RESOURCE	SOURCE	IDENTIFIER
Primers for detecting *chodl* and *beta-actin* mRNA, see Table S2	This paper	N/A
Primers for generating the plasmids used in this paper, see Table S3	This paper	N/A
Recombinant DNA		
pCMV-MCS	Susanne Schoch, University of Bonn, Germany	N/A
pDISPLAY	Aydin et al., 2012	N/A
pminiTol2	Balciunas et al., 2006	Addgene Plasmid #31829
pT3TS-Tol2	Balciunas et al., 2006	Addgene Plasmid #31831
gRNA scaffold vector pT7-gRNA	Jao et al., 2013	Addgene Plasmid #46759
pCS2-nCas9n	Wenbio Chen	Addgene Plasmid #47929
pCS2P+	Marc Kirschner	Addgene Plasmid #17095
pCS-ColXIXeGFP-DEST	Hilario et al., 2010	N/A
hsp70l:*col12a1a*-p2A-cerulean	Wehner et al., 2017	N/A
Software and Algorithms		
ImageJ	Schneider et al., 2012	https://imagej.nih.gov/ij/
GraphPad Prism 8.1.2	GraphPad Software Company	https://www.graphpad.com/scientific-software/prism/
WIS-NeuroMath software	Rishal et al., 2013	https://biii.eu/wis-neuromath
NMJ-morph	Jones et al., 2016	https://datashare.is.ed.ac.uk/handle/10283/2113
pClamp 10	Molecular Devices	https://moleculardevices.box.com/s/l8h8odzbdikalbje1iwj85x88004f588
Noldus behavior analysis set-up, EthoVision software (v. 7)	Noldus Company	https://www.noldus.com/animal-behavior-research/products/ethovision-xt
ZenBlue2.3 software, Zeiss	Carl Zeiss Company	https://www.zeiss.com/microscopy/int/home.html?vaURL=www.zeiss.com/microscopy
Odyssey Fc Imaging system and Image Studio Lite (v. 5.2)	Li-Cor Corporate Company	https://www.licor.com/bio/image-studio-lite/
GXCAM 1.3 camera with GX Capture software	GT Vision Company	https://www.gtvision.co.uk/epages/es141397.sf/en_GB/?ObjectPath=/Shops/es141397/Categories/Cameras_for_Microscopes/GXCAM_Camera_Drivers
G*Power 3.1	Faul et al., 2009	https://gpower.software.informer.com/3.1/
LightCycler® 96 Instrument Software Version 1.1.1 (Roche)	Roche Life Science Company	https://lifescience.roche.com/en_gb/brands/realtime-pcr-overview.html#software
Other		
Vivaspin 20-50000 MWCO	GE Healthcare	Cat# 28-9323-62

LEAD CONTACT AND MATERIALS AVAILABILITY

Further information and request for resources should be directed to and will be fulfilled by the Lead Contact, Thomas Becker (thomas.becker@ed.ac.uk). This study did not generate new unique reagents.

EXPERIMENTAL MODEL AND SUBJECT DETAILS

Sources of zebrafish, mouse models, and cell culture used in this study are reported below and in the Key Resources Table.

Zebrafish

All fish were kept and bred in our laboratory fish facility according to standard procedures (Westerfield, 2000), and all experiments have been approved by the British Home Office (project license no.: 70/8805). Fish lines used were the WIK wild-type strain of zebrafish and the *Tg (mnx1:GFP)* (previously *HB9:GFP*) (Flanagan-Steet et al., 2005) transgenic line. Further transgenic lines and mutants were generated using CRISPR/Cas9 and Tol2 transgenesis as described below. These lines are *chodl*−/−, and *chodl*−/−;*mnx1:chodl-FLAG*.

Mouse

The *Chodl* mutant mouse was generated as part of the IMPC project (https://www.mousephenotype.org/), designated Chodl$^{em1(IMPC)H}$, and maintained on a C57BL/6NTac background. All mouse experiments were carried out under UK Home Office project license no. PDFEDC6F0. For *ex vivo* electrophysiology experiments, 4 control (2 males and 2 females) and 6 *Chodl* mutant (3 males and 3 females) mice were used. For primary motor neuron culture, 3 control (2 males and 1 female) and 3 *Chodl* mutant (2 males and 1 female) mice were used.

Cell culture

HEK293T cells were used in this study for biochemical assays. Cells were cultured in DMEM medium supplemented with 10% fetal bovine serum (FBS), 1X Penicillin-Streptomycin (Life Technologies) at 37°C and 5% CO2 levels.

METHOD DETAILS

Plasmids for zebrafish

To generate the plasmids used in various experimental procedures the following vectors were used mammalian expression vectors pCMV-MCS, kindly provided by Susanne Schoch-McGovern, Bonn, Germany; pDISPLAY, kindly provided by Jeffrey Lee, Toronto, Canada (Aydin et al., 2012); pminiTol2, a gift from Stephen Ekker, Addgene plasmid # 31829 (Balciunas et al., 2006); gRNA scaffold vector pT7-gRNA, agift from Wenbiao Chen, Addgene plasmid # 46759 ;and pCS2P, a gift from Marc Kirschner, Addgene # 17095. All restriction enzymes and buffers used were from New England Biolabs. A full list of primers is provided in Table S3 and S1.

The zebrafish full-length *chondrolectin* (*chodl*) was obtain by PCR using pCS2-chodl-myc as template (forward EcoRI 5′- GCG GAA TTC AAC ATG CGC GCG ACA CTC AGG - 3′and reverse XhoI-FLAG 5′- GCG CTC GAG TCA TTT ATC ATC ATC ATC TTT ATA ATC TGG TCC TGG GAC CTC CAT GCC ACT GTC - 3′) and subcloned into the EcoRI-XhoI-digested CMV-MCS vector (pCMV-chodl-FLAG). Generation of truncated versions was achieved by PCR using the same forward primer as for full-length chodl and two different reverse primers (XhoI-FLAG 5′- GCG CTC GAG TCA TTT ATC ATC ATC ATC TTT ATA ATC TGG TCC TGG CAA CAT CTG GAA ACA GCA CG-3′ and XbaI –FLAG 5′-GCG TCT AGA TCA TTT ATC ATC ATC ATC TTT ATA ATC TGG TCC TGG GAC CTC CAT GCC ACT GTC-3′). PCR fragments were ligated into CMV-MCS vector digested with EcoRI and XhoI (pCMV-chodl w/o intracellular domain-FLAG), and EcoRI and XbaI (pCMV-chodl w/o CTLD-FLAG).

The zebrafish full-length *col19a1* sequence was amplified from pCS-ColXIXeGFP-DEST (gift from Christine Beattie, Ohio, US) using the following primer sets: forward (ClaI) 5′-GCG ATC GAT ACC ATG TTT TCA AGG GGC CCT TTC-3′ and reverse (XbaI-HA) 5′-GCG TCT AGA CTA AGC GTA ATC TGG AAC ATC GTA TGG GTA TGG TCC GGG GCC ATC CCG TCT ACC ATA AG-3′, and forward (SfiI) 5′- GCG GGC CCA GCC GGC CGA GAG AAT AGA TCA TAC ATG TCC-3′ and reverse (SacII) 5′-GCG CCG CGG CTA GCC ATC CCG TCT ACC ATA AG-3′. ClaI-XbaI-digested and SfiI-SacII-digested *colXIXa1* PCR fragments were subcloned into CMV-MCS vector (pCMV-*co19a1*-HA) and pDISPLAY vector (pDISPLAY-HA-*col19a1*), respectively. The TSPN domain of *col19a1* was obtained by PCR (forward 5′- GCG GGG CCC AGG AGA GAA TAG ATC ATA CAT GTC C-3′ and reverse 5′- GCG CCG CGG CTA TGC TGT GGG GTT GTG GGT C-3′) and subcloned into the ApaI-SacII-digested pDISPLAY vector (pDISPLAY-HA-TSPN). To generate the pDISPLAY-HA-NC-ColI plasmid, the NC-ColI region was digested with BglII and NotI from pDISPLAY-HA-*col19a1* and religated into pDISPLAY vector.

For the construction of pCMV-*colXIIa1*-HA the MCS of pCMV-MCS vector was replaced by a new cloning site containing the SbfI and NheI restriction enzyme sites, and the HA-tag sequence (forward EcoRI 5′- AAT TCC CTG CAG GCC CTT AAG CCC GCT AGC CCC GGA CCA TAC CCA TAC GAT GTT CCA GAT TAC GCT TAG G-3′ and reverse BamHI 5′- GAT CCC TAA GCG TAA TCT GGA ACA TCG TAT GGG TAT GGT CCG GGG CTA GCG GGC TTA AGG GCC TGC AGG G-3′). Full-length zebrafish *col12a1a* CDS was cut from the previously described hsp70l:*col12a1a*-p2A-cerulean construct (Wehner et al., 2017) and religated into the SbfI-NheI new CMV-MCS digested vector.

The mnx1 promoter was amplified from genomic DNA using the forward primer (NotI) 5′- GCG GCG GCC GCC CAT TTA AAT TAG CCT GGC ATC TGG AC-3′ and reverse primer (EcoRI) 5′-GCG GAA TTC TCT GGC CCA CCT CAC AAA CAG-3′), and the fragment was cloned into the NotI-EcoRI pminiTol2 digested vector (pminiTol2-*mnx1*). The *chodl*-FLAG-SV40pA fragment, amplified from the pCS2P-*chodl*-FLAG (forward EcoRI 5′- GCG GAA TTC AAC ATG CGC GCG ACA CTC AGG-3′ and reverse EcoRV 5′- GCG GAT ATC AAA AAA CCT CCC ACA C-3′), was sub-cloned into the EcoRI-EcoRV-digested pminiTol2-*Mnx1* vector. The pCS2P-*chodl*-FLAG plasmid was generated by amplifying the *chodl* coding sequence from pCMV-*chodl*-myc, adding an artificial Kozak sequence (AAC) 5′ of the start site and adding a Gly-Pro-Gly linker and a synthetic FLAG tag to the 3′end (forward EcoRI 5′-GCG GAA TTC AAC ATG CGC GCG ACA CTC AGG-3′ and reverse XhoI 5′-GCG CTC GAG TCA TTT ATC ATC ATC ATC TTT ATA ATC TGG TCC

TGG GAC CTC CAT GCC ACT-3′). The amplified *chodl*-FLAG fragment was digested and ligated into the EcoRI-XhoI-digeste pCS2P+ vector.

To generate chodl w/o intracellular domain (ID), the *chodl* coding sequence until the transmembrane domain (TMD) was amplified and a linker with FLAG-tag added, using the pCS2P-*chodl*-FLAG as template (forward EcoRI 5′-ATG CGA ATT CAA ACA TGC GCG CGA CAC TCA GG-3′ and reverse XhoI 5′-GCA TCT CGA GTT ACT TGT CGT CAT CGT CTT TGT AGT CAG GGC CAG GGA AAC AGC ACG TCC CTG AAG-3′). This fragment was sub-cloned into the pCS2P+ vector and used as a PCR template to add the SV40 sequence for ligation into the pminiTol2-*mnx1* plasmid (forward EcoRI 5′-GAT TCG AAT TCA AAC ATG CGC G-3′ and reverse EcoRV 5′-CGA TGA TAT CAA AAA ACC TCC CAC ACC TCC C-3′).

To generate an expression vector for Chodl w/o C-type lectin domain (CTLD), two intermediate *chodl* fragments were generated 5′ and 3′ of the CTLD (Cassette 1 forward EcoRI 5′-ATG CGA ATT CAA ACA TGC GCG CGA CAC TCA GG-3′ and reverse XhoI 5′-GCA TCT CGA GCA CTG TCT GAC CGC TCA CAA 3′, and Cassette 2 forward XhoI 5′-ATG CCT CGA GTA TGA ACC AGA AAG TCA TCT GG-3′and reverse XbaI 5′-GCA TTC TAG ATT ACT TGT CGT CAT CGT CTT TGT AGT CAG GGC CAG GGA CCT CCA TGC CAC-3′). The PCR products were ligated together into the digested pCS2P+ vector, and then the whole *chodl* cassette and SV40 amplified to ligate into pminiTol2-*mnx1* vector. The primers for this amplification are the same as previously used to generate the final cassette of the *chodl* w/o ID.

To generate chodl w/ ST- > A ID, the intracellular sequence 3′ of the transmembrane domain was mutagenized using PCR primers. A sequence of 4 primers were used, which first bound to the TMD and added 30bp of mutagenized sequence, then bound to the last 20bp of each successive mutagenized sequence and added another 30bp. The final primer also contained the Gly-Pro-Gly linker and FLAG-tag sequence. In each case, the forward primer was the same. Forward EcoRI 5′-ATG CGA ATT CAA ACA TGC GCG CGA CAC TCA GG-3′, Reverse 1 5′-AGC TTT AGC CCG TGG TTT AGC CTT AGC CAA CAT CTG GAA ACA GCA CGT CCC TGA AG-3′, Reverse 2 5′-CGT CTT AGC GAT CCA GAG AGC AGC TTG GTT GAC AGC AGC TTT AGC CCG TGG TTT AGC-3′, Reverse 3 5′-GAC CTC CAT GCC AGC GTC TAT CTT AGC CGT CTT AGC GAT CCA GAG AG-3′, Reverse 4 5′-GCA TCT CGA GTT ACT TGT CGT CAT CGT CTT TGT AGT CAG GGC CAG GGA CCT CCA TGC CAG CGT C-3′. As described for the other truncated constructs, the cassette was ligated into the pCS2P+ vector and re-amplified with the SV40 sequence, and ligated into the pminiTol2-*mnx1* vector.

To generate the pminiTol2-*mnx1*-LifeactEGFP plasmid, the LifeactEGFP fragment was generated by PCR (Forward EcoRI 5′- GCG GAA TTC AAC ATG GGA GTA GCA GAC CTA ATC-3′ and Reverse EcoRV 5′- GCG GAT ATC TAA GAT ACA TTG ATG AGT TTG GAC-3′) and ligated into the pminiTol2-*mnx1* vector. All generated plasmid were fully or partially sequenced.

Generation of a chodl mutant zebrafish

Three gRNAs targeting exon 1 of *chodl* were designed using http://zlab.bio/guide-design-resources (Ran et al., 2013). The top guides were selected for estimated cutting efficiency and fewest off-target sites, and for a restriction site to use in genotyping. Oligonucleotides for these gRNA sequences were generated using http://ZiFit.partners.org/ website to insert into the pT7-gRNA expression vector. Oligos were annealed and ligated into the pT7 vector as described elsewhere (Jao et al., 2013).

gRNA was transcribed using the mMessage mMachine T7 Transcription kit (Thermo Fisher) after the plasmids were linearized with BamHI. gRNAs were purified using the mirVana miRNA Kit (Thermo Fisher). The Cas9 mRNA was prepared from the pCS2-nCas9n plasmid (gift from Wenbiao Chen, addgene plasmid #47929), linearized with XbaI and transcribed using the mMessage mMachineT3 Transcription Kit. Each gRNA was co-injected with *cas9* mRNA into single-cell *mnx1*:GFP embryos, at an injection volume of 1nl. The final injected gRNA concentration was 15 ng/ul and the Cas9 mRNA concentration was 150 ng/ul.

At 24 hpf, the embryos were checked for normal gross morphology and motor axon appearance. In each injection clutch, 5 embryos were pooled for DNA extraction and genotyping to determine cutting efficiency of the gRNA target sequence. G0 injected fish for gRNA1 were raised and outcrossed into the WIK wild-type fish line. F1 adults were fin-clipped and genotyped for heterozygous mutation in the target sequence. Two founders had deletions of ΔCTCA, and one with ΔACACT in exon1 of *chodl*, leading to frameshift mutations and premature stops in exon 2. The two ΔCTCA founders were incrossed and had a heterogeneous clutch of motoneuron GFP^+ and GFP^- offspring. In the *mnx1*:GFP^+ embryos, ~25% of the clutch showed a shortened axon phenotype. These phenotypically identified mutant embryos were selected and raised to generate homozygous mutant stocks, and some were taken to sequence their DNA and confirm homozygosity of the indel. For the GFP^- offspring, homozygous mutant adults were selected from their non-homozygous siblings by genotyping through fin-clipping. The shortened axon phenotype in these fish was later confirmed by SV2 staining in their offspring.

Generation of trasngenic zebrafish line

chodl mutant embryos were injected at the single-cell stage with 1nl of a mixture of transposase mRNA (50ng/μl, pT3TS-Tol2, gift from Stephen Ekker, Addgene plasmid # 31831) and pminoTol2-*mnx1*:chodl-FLAG (25ng/μl) dissolved in RNase-free water. At 24 hpf, embryos were selected that showed a mosaic rescue of axon lengths. These fish were raised and backcrossed into the *chodl* mutant line, with F1 embryos selected that showed rescue of virtually all motor axons at 24 hpf. Transmission of the *mnx1*:chodl-FLAG transgene was also confirmed using FLAG immunohistochemistry on the embryos at 24 hpf.

Zebrafish DNA extraction and genotyping

Embryos were digested whole using a solution containing 2.5ul Proteinase K (Invitrogen), 10 μl Taq polymerase buffer (New England Biolabs), and 90 μl water. Embryos were heated to 65°C for 20 min, homogenized, and then heated to 95°C for 15 mins. The solution was then homogenized again, spun down and 40ul of supernatant were removed for use as a PCR template.

Adult zebrafish fins were cut by first anaesthetising the fish in 1:1000 MS-222 (Sigma) and cutting off a small portion of fin using a clean scalpel blade. The fin was digested in the same buffer as the embryos above and heated in the same sequence as for embryo DNA extraction.

The DNA was amplified using genotyping primers which span a ~300bp region around the gRNA target sequence. The amplicons were digested with the restriction enzyme for each target and run on a 2% agarose gel with the undigested amplicon. An undigested band demonstrates destruction of the restriction site via indel mutations by the Cas9. For gRNA1, which was used to generate the *chodl* mutant line, the genotyping primers are: forward 5′-GAC TGG AGC AAG TCT GTG-3′ and reverse 5′-CTG CAC GAG ACC AGA AAA-3′, with BspCNI as the restriction site.

Zebrafish qRT-PCR

mRNA was extracted from 28 hpf zebrafish embryos (100 embryos/group/experiment) according to the manufacturer's instructions (RNeasy Mini Kit, QIAGEN). cDNA was synthesized using the iScript cDNA Synthesis Kit (Bio-Rad). Reverse transcription-PCR was performed using the following pair of primers (Table S2) flanking a 232bp region between exon 5 and 7: 5′-ACCACCCACTGATGAG GATG-3′ and reverse 5′- GACCTCCATGCCACTGTCTA-3′. Beta-actin was used as loading control (forward 5′- CACTGAGGC TCCCCTGAATCCC-3′, reverse 5′- CGTACAGAGAGAGCACAGCCTGG-3′). All the amplicons were run a 1.5% agarose gel. qRT-PCR was performed using the SsoAdvanced Universal SYBR Green Supermix kit according to the manufacturer's instructions (BioRad). Samples were run in triplicates on a LightCycler 96 instrument (Roche). The data wwereas analyzed using the LightCycler 96 application software v1.1 (Roche). Expression level of *chodl* was normalized to beta-actin control.

Double-morpholino injections in zebrafish

Approximately 1 nL of morpholino solution was injected into the yolk of *mnx1:GFP* transgenic animals and motor axon morphology was evaluated as shortened or not at 24 hpf, as described (Zhong et al., 2012). Morpholino doses were titrated to be subthreshold for phenotype generation (shortened axons). Total morpholino load per egg was kept constant by filling up with standard control morpholino (GeneTools, Philomath, OR, USA).

Acute rescue assays of motor axon length in zebrafish

25ng/μl of plasmid coding for Chodl without ID (pminiTol2-*mnx1*:chodl-FLAG w/o ID), Chodl without CTLD (pminiTol2-*mnx1*:chodl-FLAG w/o CTLD) or Chodl with mutated residues in the ID (pminiTol2-*mnx1*:chodl-FLAG ST- > A) was co-injected with 50ng/μl mRNA transposase (pT3TS-Tol2) into *chodl* mutant embryos at the single-cell stage (final volume: 1 nl). As negative control for microinjection, empty pminiTol2-*mnx1* was used, while pMiniTol2-*mnx1*:chodl-FLAG was used as positive control for rescue. At 28hpf, the embryos were dechorionated, fixed, and immunohistochemistry for GFP and FLAG was performed. Axon length was measured using ImageJ, presence of FLAG expression was determined by fluorescence microscopy. Axons were only considered FLAG positive if the FLAG staining was visible along the full length of the axon, if the neuronal morphology matched that of the CaP neuron, with its soma situated directly above the peripheral axon, as described (Myers et al., 1986). This avoided mistakenly measuring motor axons from RoP or MiP primary motor neurons. Images were analyzed in a blinded fashion.

Zebrafish whole-mount immunohistochemistry

Between 24 and 30 hpf, the zebrafish embryos were dechorionated and fixed for 45 min at room temperature in 4% PFA / 1% DMSO. This under-fixation is necessary to detect the low signal in the synapse preparations and the injected FLAG constructs. The embryos were then rinsed 3x5mins with PBS + 0.1% Triton X-100 and blocked using blocking buffer containing 1% normal donkey serum (1% DMSO, 1% BSA, 0.7% Triton X-100 in PBS pH 7.4) for 60 – 90 min at room temperature with gentle shaking. The embryos were then incubated overnight at 4°C with the primary antibodies in blocking buffer with 1% normal donkey serum. Primary antibodies were: anti-GFP (1:400, AbCam, AB13970), anti-FLAG (1:100, Sigma, F1804), anti-SV2 (1:200, DSHB), anti-Znp-1 (1:100, DSHB) and anti-AChR (1:200, DSHB, mAb35). The primary antibodies were washed off using PBS-Tx for 6 × 10 min and the secondary antibody incubated for 4 h at room temperature. Secondary antibodies used were: AlexaFluor488 donkey anti-chicken (1:400, Jackson ImmunoResearch), AlexaFluor 594 donkey anti-mouse (1:400 Jackson ImmunoResearch), AlexaFluor 594 donkey anti-mouse with pre-adsorption against rat protein (1:400, Jackson ImmunoResearch), AlexaFluor 488 donkey anti-rat with pre-adsorption against mouse protein (1:400, Jackson ImmunoResearch) and AlexaFluor 647 donkey anti-rat with pre-adsorption against mouse protein (1:400, Jackson ImmunoResearch). After fully rinsing off the secondary antibody, the embryos were settled in 70% glycerol / 30% PBS and stored wrapped in foil at 4°C until imaging.

At 3dpf, the larvae were fixed in 4% PFA / 1% DMSO for 4 h at 4°C. After 3 × 10 min rinsing in PBS + 0.1% Triton X-100, the larvae were skinned to make the muscle more accessible to antibody labeling. The larvae were fixed to a silicone-coated Petri dish with insect pins and most of the liquid sucked away from the larvae. Sharpened tungsten wire was used to gently pull the skin away from the head area, and fine forceps were then used to fully pull the skin off the trunk and tail. After skinning, the larvae were incubated

for 60 - 90 min in blocking buffer as described above at room temperature. Primary and secondary antibodies were used at the same concentrations and incubation time as described for the embryos.

Zebrafish phalloidin staining and analysis

At 30 hpf, zebrafish embryos were dechorionated and fixed overnight at 4°C. After washes with PBS+Tween (0.1%), the embryos were permeabilised by incubation in PBS+Triton X-100 (2%) for 2 h at room temperature. After further brief washes in PBS + 0.1% Tween-20, the embryos were incubated in PBS + 0.1% Tween + 5% AF568 Phalloidin (Thermofisher). After washing using PBS+0.1% Tween-20, the embryos were settled in 70% glycerol / 30% PBS before imaging.

A single optical plane was analyzed which showed the full somite, and the number of distinct muscle cells per somite counted. The average width of each muscle cell was also measured. For each embryo, images of three somites were analyzed with the observer blinded to the genotype.

Zebrafish whole-mount confocal imaging

All zebrafish were mounted onto glass slides using 70% glycerol, deyolked with insect pins, and covered with coverslips anchored with silicone gel. Images were acquired using a Zeiss LSM880 Indimo, Axio examiner confocal microscope with Plan-Apochromat 20x/0.8 objective.

Synaptic puncta quantification in zebrafish

All measurement of the synaptic puncta, labeled by SV2, Syt2 and AChR antibodies, was performed in ImageJ (Schneider et al., 2012). For analysis, an approximate 400 μm^2 square (20x20) was drawn around the horizontal myoseptum in 28 hpf embryos, with 4 - 5 axons measured and the values averaged for each embryo. To determine synaptic measurements in the axonal branches at 3 dpf, a 1600 μm^2 square (40x40) was drawn in the ventral region of the myotome, with the top edge of the ROI 40 μm ventral to the horizontal myoseptum, with 3 myotomes averaged per larva.

In each square, the synaptic compartment was analyzed by performing background subtraction of the images, with a rolling ball radius of 33% of the square's length in pixels. A 30% threshold was applied to all channels. Threshold values were calculated from the maximum gray value measured from a smoothed duplicated image. After application of the threshold, the Analyze Puncta function was used to count puncta number and area (outline mask was generated). The minimum area defined as a punctum for the Analyze Particle function was set as 0.6 μm^2. This was qualitatively determined as the minimum size to remove background noise without loss of true puncta.

The outline mask was used to create a ROI mask. The ROI mask was applied on the raw images (after background subtraction) and the mean gray value was measured. The observer was blinded to the experimental condition before measuring.

Time-lapse imaging of axon filopodia in zebrafish

Embryos containing *mnx1*-LifeactEGFP expressing CaP axons were mounted in 1 - 1.2% low melting agarose with 0.01% tricaine (MS-222). Images were acquired using a Zeiss LSM 880 confocal laser scanning microscopy with Airyscan and a Plan-Apochromat 20x/0.8 objective. Z stack (space 0.500 μm) were collected every 30 s over a period of 60 min. Fiji software was used to quantify the number and the lifetime of filopodia in each frame of each time-lapse sequence. The lifetime of filopodia was defined as the length of time for which its presence was detected during imaging. Three wild-type and three *chodl* mutants were analyzed (one axon/fish). The observer was blinded to the genotype while performing measurements.

Analysis of MiP motor axons in zebrafish

33hpf zebrafish embryos were fixed and stained for endogenous EGFP (anti-GFP, 1:400, AbCam, AB13970) and znp-1 (anti-Znp-1, 1:100, DSHB). Secondary antibodies used were: AlexaFluor488 donkey anti-chicken (1:400, Jackson ImmunoResearch) and AlexaFluor 594 donkey anti-mouse with pre-adsorption against rat protein (1:400, Jackson ImmunoResearch). Images were acquired using a Zeiss LSM880 Indimo, Axio examiner confocal microscope with Plan-Apochromat 20x/0.8 objective. Five to six MiP motor axons per embryo were scored for extending beyond the dorsal border of the spinal cord, as described (Zhong et al., 2012) . During measurements the observer was blinded to the genotype.

Zebrafish larval behavior analysis

To analyze swimming distance, 3 dpf larvae were touched on the median fin fold with a fire-pulled pipette. The swim path of their escape response was recorded and analyzed using a Noldus behavior analysis set-up and EthoVision software (v. 7). Behavioral data are shown as distance traveled within 15 s after touch, averaged for triplicate measures per larvae.

To measure turning angles, we recorded larvae using a Casio EX-ZR1300 camera with high-speed recording set to 1000 frames / second. Larvae were recorded before, during, and after an escape response from a head tap with a fire-pulled glass pipette. The larvae were touched on the tip of their nose and they subsequently turned randomly to the left or right to escape the stimulus. The angle of the initial escape after the C-bend was binned into 45° segments from the starting position without considering the direction of the bending. The escape response was recorded in triplicate per larva.

To analyze the number of spontaneous contractions, 18-19hpf embryos were recorded continuously for 5 min under a stereomicroscope equipped with a GXCAM 1.3 camera and the number of coiling movements counted. The videos were recorded using the GX Capture software at a speed of 6.2-5.3 frames/second (resolution 1272x952).

All behavioral experiments and analyses of videos were done in a blinded fashion.

Genotyping PCR for mice

Genomic DNA (gDNA) was prepared using PureLink Genomic DNA Kit (Invitrogen) according to the manufacturer's instruction. Founder mice were identified by genotyping PCR using HotStarTaq DNA polymerase (QIAGEN) with 2 gene-specific primer pairs (pair A: 5′- ACGTGAGTTTAGAGGGAAAGTTTG −3′ and 5′- CAGGATTGGCAGTTGGTTGGT −3′; pair B: 5′-GGCTGGCTTGT GAAAGTGAAG-3′ and 5′-GTTTGGCCATCTCCGCTTCT-3′). Both the primers were used for routine genotyping.

Mouse primary motor neuron cell culture

Primary motor neurons were isolated from the lumbar spinal cords of E12.5-13 WT and *Chodl* −/− homozygous embryos by using a p75NTR-panning protocol (Wiese et al., 2010). Briefly, the lumbar region (L1-L6 segment) of the spinal cord was dissected from each embryo and enriched on laminin and Poly-dl-ornithine hydrobromide (Sigma) -coated plates in neurobasal medium (Invitrogen) containing GlutaMAX I supplemented with 10% heat-inactivated horse serum (Sigma) and 5 ng/ml brain derived neurotrophic factor (BDNF; PeproTech) and ciliary neurotrophic factor (CNTF; PeproTech). Motor neurons were plated till 5 days *in vitro*. The cells were fixed with 4% paraformaldehyde in phosphate buffered saline (PBS) for 15 min at room temperature, washed three time with PBS 1X for 5 min, and stored at 4◦C.

Immunohistochemistry

The samples were incubated with the immunofluorescence (IF) blocking buffer (0.01% Triton X-100/TBS and 10% normal serum) for 1 h at room temperature and washed once with IF buffer (0.01% Triton X-100/TBS). After blocking, the cells were incubated overnight at 4°C with the primary antibodies diluted in IF buffer: rabbit anti-Tuj1 (Covance, 1:2000) and mouse anti-Islet1 (DSHB, 1:50), After washing steps the cells were incubated for 1 h at room temperature with the appropriate secondary antibodies: Alexa Fluor 488 and Alexa Fluor 568 (Invitrogen, 1:500), washed twice and counterstained with DAPI for nucleus staining before mounted with Vectashield Hard Set (Vector) Mounting Medium. Fluorescence was visualized using a confocal microscope Zeiss LSM.

Quantifications

All measurements of the neuronal morphologies were performed using automated WIS-NeuroMath software (Rishal et al., 2013). Neurite lengths, branching, cell body area and other parameters were calculated and saved for each cell, while ignoring neurites which were not attached to cell bodies or attached to excessively small or large cell bodies. The cell body size was calculated using threshold-based segmentation using the same software.

Ex vivo electrophysiology in mice

Experimental procedures on 4 months-old mice were performed as described previously (Webster et al., 2013). Phrenic nerve/hemidiaphragm preparations were bathed in Krebs-Henseleit buffer: 95% O_2 / 5% CO_2. Experiments took place in a Faraday enclosure at room temperature (20 – 22°C). Phrenic nerve was stimulated with a solid-state square wave pulse generator (Grass Instruments, Quincy, MA, USA) via a suction electrode. The signal was amplified using an Axoclamp 900A amplifier (Molecular Devices, Sunnyvale, CA, USA). Compound muscle action potential (CMAP; example traces in Figure S7I-K) was recorded with a low resistance extracellular glass electrode, containing bath solution, placed close to central area of the muscle. Recordings of CMAPs were made prior to blockade of muscle sodium channels. Blockade of muscle contraction was achieved with 2.5 μM μ-conotoxin GIIIB (Alomone labs, Jerusalem, Israel). A borosilicate glass electrode (10–15 MΩ resistance, filled with 3M KCl) was used for recording miniature endplate potentials (MEPPs) and evoked endplate potentials (EPPs) from individual muscle fibers. A micromanipulation rig (Scientifica, Maidenhead, UK) was used to place electrodes as near to the endplate region as possible, with visualization under a BX51WI stereomicroscope (Olympus, Southend-on-Sea, UK). Recordings were analyzed using pCLAMP 9 software (Molecular Devices), and normalized to a −80 mV baseline, thus correcting for differences in resting membrane potential. For each preparation 12-15 fibers were impaled, ∼30 mEPPs over were acquired and averaged. EPPS were recorded at 1 Hz stimulation frequency, 20 EPPS were acquired and averaged for each fiber. Data from each preparation (up to 15 fibers) were averaged, each n represents a single preparation. For determination of quantal content, EPP amplitude was subjected the further species-specific correction, as follows:

$$AMP_{EPP} = AMP_{EPP\ (measured)} \Big/ \left[1 - 0.8\ AMP_{EPP\ (measured)} \Big/ E\right]$$

Where AMP_{EPP} is the EPP amplitude, 0.8 the correction factor for mouse endplates, and E the resting membrane potential (−80 mV). Quantal content was calculated according to the following formula:

$$\text{Quantal content} = \text{mean}(AMP_{EPP}) / \text{mean}(AMP_{MEPP})$$

Where AMP_{MEPP} is the MEPP amplitude.

The experimenter was blinded to genotype of animals during acquisition and analysis of data.

Mouse muscle preparation and immunohistochemistry

Mice were sacrificed, muscles dissected, and neuromuscular junctions immunohistochemically labeled and observed as previously described (Sleigh et al., 2014b). Muscles were dissected in cold 1 × phosphate-buffered saline (PBS) and fixed in 4% (w / v) paraformaldehyde in PBS (PFA, Electron Microscopy Sciences) for 15 min. Initially the muscles were permeabilized with 2% Triton X-100 in PBS for 30 min, before blocking in 4% bovine serum albumin and 1% Triton X-100 in PBS for 30 min and then incubated overnight at 4°C in blocking solution with appropriate primary antibodies against neurofilament (2H3, 1/50, DSHB); synaptic vesicles (SV2, 1/100, DSHB); mouse anti-bassoon, 1:500 (cat. no. GTX13249, SAP7F407, Source BioScience, Nottingham, UK); rabbit anti-piccolo, cat. no. 142002, 1:200, and rabbit anti-P/Q-VGCC (Cav2.1), cat. no. 152203, 1:300 (Synaptic Systems, Göttingen, Germany). The next day, muscles were washed three times with PBS before a 2-hours incubation with secondary antibodies (1:250, Invitrogen, varieties of Alexa Fluor-488 conjugated, −568-conjugated and 1.5 mg/ml tetramethylrhodamine (TRITC) a-BTX (Cambridge Bioscience) in PBS. Finally, muscles were washed three times in PBS for 30 min and mounted in hard set Vectashield (Vector labs) on glass slides with DAPI for confocal imaging.

Images were acquired using a Zeiss LSM 710 confocal microscope. Morphometric analysis of neuromuscular junctions was carried out using a standardized platform: ''NMJ-morph'' (Jones et al., 2016). *In vivo* axon branching was measured from processed binary images generated in ImageJ. Pixel positions of skeletonized images were used in quantifying branching patterns using a binary connectivity plugin. Experiments were done blinded with mice identified only by codes and earclip number until all testing was completed.

Behavioral analysis in mice

Open field testing was performed using PAS Homecage (San Diego Instruments) for a period of 20 min. The means of two trials were analyzed per time point. Accelerating rotarod (Med Associates; 4–40 rpm) was performed to a maximum trial length of 300 s. Tested 2 times each day, over 3 separate days (2 × 3), average of 6 replicates used for final analysis.

The four-limb hanging wire test was conducted using a 43 cm^2 grip-grid secured above a padded surface. Each trial was performed for a maximum of 120 s, or until the mice fell before the time was up. The mean of six trials per mouse was analyzed per time point. Behavioral testing was performed at monthly intervals without knowledge of the genotype.

HEK293T transfection and binding assays

HEK293T cells were platted at a density of $1.5x10^5$ cells / 100 mm dish and transfected with 8 - 10 μg plasmid DNA using standard $CaPO_4$ transfection (Kwon and Firestein, 2013).

For immunofluorescence experiments, HEK293T cells were plated on poly-D-lysine coverslips and transfected with 0.5 μg plasmid DNA using Lipofectamine2000 (Invitrogene) according to the manufacturers' instructions. At 24 h post-transfection, the medium was replaced with serum-free medium containing ColXIXa1 or ColXIIa1a, and further incubated for 24 h.

Immuno-labeling of transfected HEK293T cells

For immunostaining of Chodl, *col19a1* and *col12a1a*, transfected HEK293T cells were fixed for 10min in 4% PFA / 4% glucose, permeabilized (0,3% Triton X-100 in PBS) and blocked for 1 h at room temperature in blocking solution (1% BSA, 1% NGS, 0.1x Triton X-100 in PBS). Cells were incubated overnight at 4°C in primary antibodies (anti-HA, 1:400, BioLegend, Clone 16B12, and anti-FLAG 1:200, Cell Signaling, D6W5B). Following the washing steps, cells were incubated for 40 min at room temperature in secondary antibodies (1:400, Alexa Fluor 647 donkey anti-rabbit, Jackson ImmunoResearch, 1:400, Alexa Fluor 488 donkey anti-mouse, Jackson ImmunoResearch, and 1:400, Alexa Fluor 647 donkey anti-mouse, Jackson ImmunoResearch). Coverslips were extensively washed, mounted in Mowiol and let dry overnight before imaging. Binding at the cell surface was measured on a single plane using the profile tool from ZenBlue 2.3 software. Data were exported in Excel and the scatterplot was generated. Analysis was done on two different batches of HEK293T transfected cells. Two different coverslips per transfection batch were imaged and analyzed.

Protein binding assays

HEK293T cells transfected with FLAG-tagged constructs were lysed for 1h in ice cold lysis buffer (50mM HEPES pH7.5, 150mM NaCl, 1% Triton X-100) supplemented with proteinase inhibitors (Roche), followed by a short centrifugation step at 14000rpm / 10min / 4°C. The clear supernatant was either incubated for 1h with FLAG M2 magnetic beads (Sigma) to collect the overexpressed Chodl or directly mixed with purified HA-tagged ColXIXa1. HA-tagged ColXIXa1 was produced and secreted by HEK293T cells in the presence of 50 μg/ml ascorbic acid. The cell culture medium was concentrated using VIVASPIN concentrators (MWCO 50000), followed by purification via HA magnetic beads (Thermo Scientific). All the binding assays were performed at 4°C for 2 h on a rotator. After incubation, the beads were extensively washed with lysis buffer and boiled at 95°C / 5 min in Laemmli buffer supplemented with β-ME. Proteins were resolved in SDS-PAGE gel and transferred to nitrocellulose membrane (Bio Rad). The detection of proteins was performed using primary antibodies against HA (1:1000, BioLegend, Clone 16B12) and FLAG (1:1000, Sigma, F1804, or Cell Signaling, D6W5B), and secondary antibodies IRDye 800CW goat anti-mouse IgG (1:1000, Li-Cor) and IRDye 680LT goat anti-rabbit IgG (1:10000, Li-Cor). Membranes were scanned using the Odyssey Fc imaging system.

QUANTIFICATION AND STATISTICAL ANALYSIS

All quantitative data were tested for normality and analyzed with parametric and non-parametric tests as appropriate. For multiple comparisons, we used: One-way ANOVA with Tukey's Multiple Comparison Test (Figures 1D, 2B, 2C, 2D, 2G, 3K, 3N, 5C, S1H, and S3B), Kruskal-Wallis test with Dunn's multiple comparison test (Figures 1B, 2E, 2F, 2H, 2I, 5F, S1M, and S3C) or two-way ANOVA with Sidak's multiple comparisons test (Figures S7A, S7B, and S7D–S7H). For single comparisons, we used: unpaired t test (Figures 4C–4N, S1E, S2C, S2E, S3E–S3O, S4C, S5E–S5H, S6C, S6E, and S6L–S6M), Mann–Whitney U tests (Figures S1F and S4E) or one sample t test (Figure 6D; Figure S1I).

Statistical power was calculated using G*Power (Faul et al., 2009) (aim for most experiments > 0.8; indicated in Figure legends). *$p < 0.05$, **$p < 0.01$, ***$p < 0.001$, ****$p < 0.0001$; n.s. indicates no significance ($p > 0.05$). Error bars indicate the standard error of the mean (SEM). The Figures were prepared with Adobe Photoshop CC and Adobe Illustrator CC/ Adobe Photoshop and Adobe Illustrator Creative Cloud. Graphs were generated using GraphPad Prism 7/GraphPad Prism 8.01.

DATA AND CODE AVAILABILITY

Original Coomassie and western blot data used to generate any of the figure panels in the paper are available on Mendeley Data (https://doi.org/10.17632/g23ts8jjpp.1).